Thermoelectric generator (TEG) technologies and applications

Hussam Jouhara[a],*, Alina Żabnieńska-Góra[a,b], Navid Khordehgah[a], Qusay Doraghi[a], Lujean Ahmad[a], Les Norman[a], Brian Axcell[a], Luiz Wrobel[a,c], Sheng Dai[d]

[a] Heat Pipe and Thermal Management Research Group, College of Engineering, Design and Physical Sciences, Brunel University London, London UB8 3PH, UK
[b] Wroclaw University of Science and Technology, Faculty of Environmental Engineering, Wybrzeze Wyspianskiego 27, 50-370 Wroclaw, Poland
[c] Pontifical Catholic University of Rio de Janeiro (PUC-Rio), Rio de Janeiro, Brazil
[d] College of Engineering, Design and Physical Sciences, Brunel University London, London UB8 3PH, UK

ABSTRACT

Nowadays humans are facing difficult issues, such as increasing power costs, environmental pollution and global warming. In order to reduce their consequences, scientists are concentrating on improving power generators focused on energy harvesting. Thermoelectric generators (TEGs) have demonstrated their capacity to transform thermal energy directly into electric power through the Seebeck effect. Due to the unique advantages they present, thermoelectric systems have emerged during the last decade as a promising alternative among other technologies for green power production. In this regard, thermoelectric device output prediction is important both for determining the future use of this new technology and for specifying the key design parameters of thermoelectric generators and systems. Moreover, TEGs are environmentally safe, work quietly as they do not include mechanical mechanisms or rotating elements and can be manufactured on a broad variety of substrates such as silicon, polymers and ceramics. In addition, TEGs are position-independent, have a long working life and are ideal for bulk and compact applications. Furthermore, Thermoelectric generators have been found as a viable solution for direct generation of electricity from waste heat in industrial processes. This paper presents in-depth analysis of TEGs, beginning with a comprehensive overview of their working principles such as the Seebeck effect, the Peltier effect, the Thomson effect and Joule heating with their applications, materials used, Figure of Merit, improvement techniques including different thermoelectric material arrangements and technologies used and substrate types. Moreover, performance simulation examples such as COMSOL Multiphysics and ANSYS-Computational Fluid Dynamics are investigated.

1. Introduction

When generating electricity in power stations, around two thirds of the energy is lost in the form of waste heat that is discharged from cooling towers [1]. The main reason is that the gas or steam-powered turbine systems, that operate to produce most of the electrical power, primarily function by burning fuel to produce energy in the form of heat. This is followed by the conversion of this heat energy into mechanical energy within the turbine, and finally turning the mechanical energy into electrical energy in a generator [2]. As a result, only about 1/3 of the energy released from the fuel actually ends up in the transmission lines leaving the power plant [3,4].

The ability to collect the heat wasted within these processes and convert it to usable electrical power would enormously increase the efficiency of power generation. Additionally, the reduction of greenhouse emission from the reduced wastage would be beneficial for the environment as less fuel is burned for the same amount of electricity produced.

In recent years, thermoelectric generator (TEG) systems have attracted great consideration in the recovery of waste heat due to their incomparable advantages [5,6]: TEGs provide an opportunity to generate electrical energy from heat energy without the need for moving parts such as turbines, which eliminates extra costs resulting from maintenance and replacement [7]. TEGs have no economy-scale-of effect and can be utilised for micro generation in a restricted position or can be used to generate kilowatts. TEGs are also environmentally favourable as they operate with no sound pollution [8]. Conversely, TEGs do have a low energy conversion efficiency and require a relatively constant heat source, which are disadvantages [9].

TEGs can be used in numerous applications, such as waste heat recovery [10] and solar energy operation, experimental measurements of solar thermoelectric generators with a peak efficiency of 9.6% and a system efficiency of 7.4% are reported by Kraemer et al.

* Corresponding author.
E-mail address: hussam.jouhara@brunel.ac.uk (H. Jouhara).

Nomenclature

Symbols and abbreviations

E	Electronic Charge
E_c	Condition Band
E_f	Fermi Level
E_v	Valence Band
I	Electrical Current (A)
k	Boltzmann's Constant
K	Thermal Conductivity (W/m*K)
P	Power Generated (W)
$\dot{Q}$	Heat Transfer Rate (W)
$\dot{Q}J$	Joule's Heating Effect (W)
QH	Thermal Energy (Hot Side) (J)
R	Electrical Resistance (Ω)
S	Seebeck Coefficient
T	Temperature (K)
V	Voltage (V)

Greek symbol

σ	Electrical Conductivity (S/m)
η	Efficiency of TEG
Δ	Difference

Abbreviations

BMEP	Different Brake Mean Effective Pressures
CFD	Computational Fluid Dynamics
DCTEG	Direct Contact Thermoelectric Generator
HEX	Heat Exchanger
PVT	Photovoltaic-Thermal
PF	Power Factor
TC	Thermo Couple
TE	Thermo Electric
TEG	Thermoelectric Generator
TEM	Thermoelectric Module
zT	Figure of Merit

Superscripts/Subscripts

C	Cold
E	Electros
L	Lattice
Elec	Electric
J	Joule
H	Hot
Max	Maximum
OC	Open Circuit
SC	Short Circuit

[11]. Bayod-Rújula et al. [12] designed and constructed presented a design and developed of an experimental installation consisting of two Photovoltaic-thermal hybrid solar collectors, one of them with integrated TEG modules. This prototype would make it possible to observe the rise in electrical efficiency that can be accomplished by introducing TEG in PVT modules . Similarly, A novel hybrid energy harvesting (EH) system consisting of a dynamic offset feed mirrored parabolic integrated solar panel with thermoelectric generator (TEG) on the lower side of the solar panel was proposed by Singh et al. [13]. The proposed energy harvesting device simultaneously absorbs both solar and thermal energy, making the system ideal as a hybrid energy harvesting system. More recent investigataion into solar thermoelectric generators can be found in references [14,15,16].

An early application was a generator for remote subsea wellheads [17]. One of their strengths is their flexibility in application as noted by the following examples. A multigeneration system combined with a thermoelectric generator based on biomass gasification equipment was introduced in a study [18]. A flexible thermoelectric generator using eutectic gallium indium liquid metal together with a high thermal conductivity elastomer was designed to harvest body heat which can then be used for wearable electronics [19,20].A triple micro combustor aimed at portable power generation was designed and developed to enhance heat transmission from hot gases to thermoelectric modules considerably [21].

2. TEG−working principle

Mostly, TEG systems consist of three key elements:

1. A heat exchanger (HEX); This absorbs the heat and transfers it into the thermoelectric modules.
2. Thermoelectric modules (TEMs); The TEMs generate electricity when a temperature difference exists between their ends. A TEM contains many pairs of thermoelectric couples, and each couple normally combines a pair of p- and n-type semiconductors.
3. A heat sink; In order to dissipate the additional heat from the thermoelectric modules.

The temperature difference between two sides of the generator is what determines the operation of TEGs. Fig. 1 explains the theory behind TEGs. If one side of a piece of metal could be heated while simultaneously cooling the other side, electrons surrounding the metal atoms at the hot side will have more energy than the equivalent electrons at the cooler side, this means the hot electrons will have more kinetic energy than those in the cooler side.

Hence, the hot electrons travel more quickly towards the cold side than the cold electrons move towards the hot side, and eventually the cold end of the thermoelectric generator becomes negatively charged, and the hot end positively charged [23].

A drawback of this technique is that the voltage generated is very small and this cannot be overcome simply by linking groups of metal parts together in sequence because, the wires used to connect them, which are also made of metals, would produce a voltage in the wrong direction and oppose the voltages produced in the main metal parts.

So the most effective way to address this issue is, to develop a material that can conduct electricity using positively charged
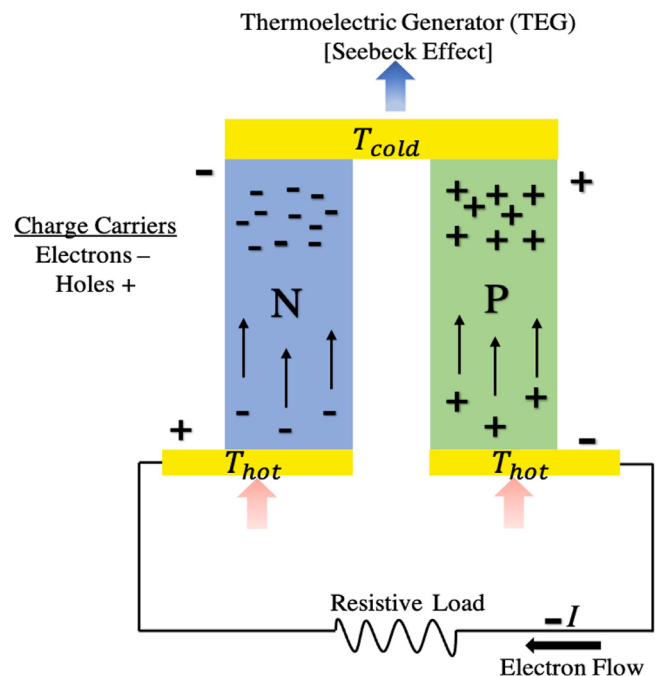

Fig. 1. Principle of thermoelectric generation [22].

particles instead of electrons, whilst, at the same time, the electrons in such materials will also assist the process by moving away from the hot to the cold side. In this case, if a chain of such new wires or materials are linked together, the voltages will add through the chain allowing a functional quantity of power to be generated by the consumer. Materials with this positive conducting property are always semiconductors [24].

A further issue regarding thermoelectric devices is that the type of materials that enable electrons to flow easily to order to generate electricity also happen to be very good heat conductors, so any temperature gradient driving the process very quickly lost and the output falls. Researchers are hence challenged to find materials with low thermal conductivity but high electrical conductivity.

A possible way of achieving this is by using metal alloys that can be used to shape a grid of differently sized atoms that slow down the heat flow whilst allowing electrons to move freely. Likewise, certain configurations of nanoparticles can trap heat and slow it down. In summary, the more joins or barriers that exist between particles, the slower the heat can move.

2.1. Seebeck effect

This mechanism, where a temperature differential produces a voltage, is known as the thermoelectric effect or Seebeck effect and it was believed to have been defined for the first time in the 1820s by the German physicist Thomas Johann Seebeck. However, recent evidence shows that Alessandro Volta had also observed the Seebeck effect 27 years before Thomas Seebeck. [25].

During an experiment carried out 1794, Alessandro Volta designed a U-shaped iron pin, in which one end of the rod was heated by dipping it in hot water. During the next step, the unevenly heated rod was electrically attached to a dead frog's leg. The current went through the frog's leg, and its muscles contracted. This is considered to be the first example of the Seebeck influence. [26].

2.1.1. Seebeck coefficient

The Seebeck effect explains the build-up of a potential gap (ΔV) through a semiconductor (or conductor) because of the diffusion of its load carriers over a temperature gradient ($\Delta T = T_{hot} - T_{cold}$). It is encountered by the substance if one side of it is heated or cooled.

Charges switch from the hot to the cold edge, contributing to a variation in the amount of charge carriers, an effect that is offset by the resultant internal electrical field. The form of carrier of the majority charge will specify the sign of the potential difference which, by definition, is identified by the potential of the cold side in relation to the hot side [27]. The Seebeck coefficient sign shows that the material is a p-type or n-type conductor, the positive sign indicates the p-type, the negative indicates the n-type material.

The Seebeck coefficient (S), which is responsible for allowing the current to move while the temperature gradient is present, is the relation between the theoretical differential created and the temperature gradient applied which may be seen in Eq. (1) [28]:

$$S = -\frac{\Delta V}{\Delta T} \tag{1}$$

The temperature gradient (ΔT) must be produced between the two sides of the sample and the resulting voltage (ΔV) must be measured by taking electrical connections from those two points (sides).

2.2. Peltier effect

As mentioned earlier, in 1821, Thomas Seebeck, a German physicist, carried out numerous tests on electricity and discovered that electricity can function through a circuit comprising two separate conductors, given that the junctions at which these conductors connected were kept at different temperatures. Seebeck, though, was
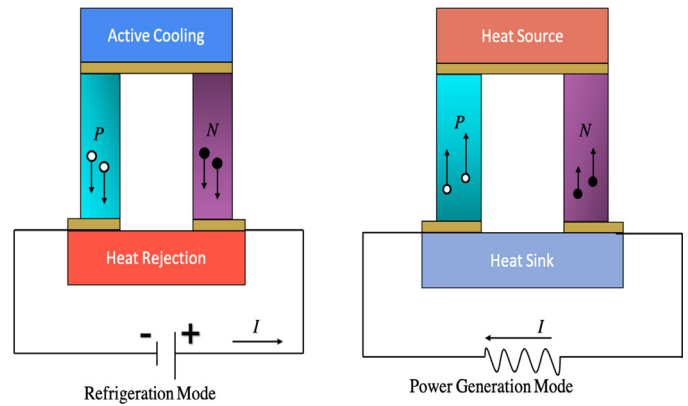

Fig. 2. Power Generation and Electrical Refrigeration (Peltier Effect) [29].

unable to clarify the real empirical hypothesis behind this process and wrongly deduced that flowing heat causes the same result as flowing energy.

Gene Peltier (a French scientist) discovered in 1834, when researching the influence of Seebeck, that heat could be consumed at one junction of dissimilar metals and emitted at the other junction of the same circuit. Then throughout the 1850s, Lord Kelvin (William Thomson), was able to theoretically validate the results of both Seebeck and Peltier and to establish the connection between them.

Nevertheless, this result was restricted to being just a laboratory-based experiment until 1930, when Russian physicists started to re-investigate earlier experiments on the thermoelectric effect, which contributed to the development of realistic thermoelectric instruments; the Peltier effect is believed to be the opposite of the Seebeck effect [29].

The electrical current passing across the junction of the two materials produces or absorbs heat per unit time at the junction to offset the gap in the chemical structure capacity of the two materials. Thanks to this influence, an electronic refrigerator, known as the Peltier cooler, can be produced.

The Peltier effect appears because the average energy of the electrons involved in the transmission of electrical current in the various conductors is different. Numerous considerations, such as the energy range of electrons, their distribution in the conductor and the atoms scattering them under the effect of applied voltage at the junction of two dissimilar conductors, will have an effect on the conductor. Fig. 2 illustrates the power generation and electronic refrigeration (Peltier effect) capabilities of the thermoelectric module.

The electrons move from one electrode to another based on the path of the electrical charge wave, then pass their extra energy to the surrounding atoms (exude) or consume energy from the surrounding atoms.

The Peltier effect is very low in efficiency which is a setback. Another downside is that the circulating current itself continues to produce a significant amount of heat which adds to the heat dissipation process. This results in an unnecessary amount of heat for large applications that, in the main, has to be managed by supplementary fans and as a consequence of this effect, a lot of energy is used, making it very costly and preventing its large-scale implementation. Furthermore, if Peltier system components become too cold, can produce a short circuit due to condensation.

The key benefit of the Peltier effect is that it allows the development of cooling and heating devices that do not involve moving parts; thus, such devices are much less prone to malfunction relative to traditional coolers and heaters and therefore do not need maintenance. Peltier devices do not generate sound when operating and can theoretically reach temperatures as low as -80°C. Usually, the Peltier effect is used productively at the microscopic level where traditional cooling techniques do not operate [30].

Commonly used devices that utilise the Peltier effect include a Peltier heater, a heat pump cooler and a solid-state refrigerator, where electrical current passing into a Peltier heater from one side of the system to another causes it to operate as a heater or a cooler. All Peltier devices operate using this method, by using electrical current to move heat from one side of the device to the other against the temperature gradient.

The Peltier effect is further used in dehumidifiers to removing moisture from the air (water extraction) and in DNA replication and synthesis where the thermal cycle uses the effect for the DNA synthesis process. In fact, astronauts also utilise the Peltier effect to counteract the uneven sunlight influence on the sides of their body, and which serves to dissipate heat from intense sunlight on one side of the astronaut to the other which, not being in direct sunlight, is much colder [31].

2.3. Thomson effect

Thomson indicated that as the current passes into unequally heated conductors, the thermal energy is either consumed or formed in the metal structure [32]. In other words, the Thomson effect is the generation of reversible heat when an electrical current is passed through a conductive material subjected to a temperature gradient [33].

The Thomson effect therefore describes the heat loss of a substance with a current through it and this transfer of heat is immediately observable. It is different from the effects of Peltier and Seebeck, for which only the net effect of two different materials can be measured.

2.3.1. Positive and negative Thomson effect

Fig. 3 shows a copper bar, as indicated from point A to B which is heated at the centre at point C. When no current is flowing through the bar, points M and N, are equidistant from C, are at the same temperature. However, when current flows from point A to B, point N indicates a higher temperature than point M. Similarly, the temperature of point B will be higher than point A. In this case, with the current flow, it can be assumed that heat is absorbed from points A to C and emitted from point C to B.

This is known as a positive Thomson effect and similar effects are observed in the case of Antimony, Silver, Zinc and Cadmium.

Conversely, in the case of iron, as the bar is similarly heated at point C and with current flowing from A to B, the temperature at point M becomes higher than that at point N, which means that the heat shifts from point C to point A and is drained from points C to point B, i.e, a negative Thomson effect. A similar effect is noticed in the case of Platinum, Bismuth, Cobalt, Nickel and Mercury [32].

2.3.2. Thomson coefficient

As a mesure of this effect, the amount of heat absorbed or evolved when one ampere of current flows for one second (i.e. one Coulomb) in a metal between two points which differ in temperature by one degree Celsius is known as the Thomson coefficient [35].

2.4. Joule heating

The heating effect was first studied and categorised by James Prescott Joule, around the year 1840. Joule set out to investigate if the recently invented electrical motor could be more efficient, in terms of cost, than the steam engines in use at the time. This led him to conduct a series of experiments on the production, transfer and use of energy and mechanical work that ultimately led to the first law of thermodynamics.

Those experiments involved studying the relationship between an electrical current that flows through a conductor and its rise in temperature. The experiment consisted of a wire submerged in water and connected to the terminals of a battery. When the circuit was closed, a rise in the water temperature could be measured. The analysis of the recorded data led to the original form of the relation now known as Joule's first law, that "the heat per second developed in the wire is proportional to the resistance of the wire and to the square of the current".

Joule heating (also known as ohmic heating) defines the process whereby the energy of an electric current is converted into heat as it flows through a resistance.

In particular, when the electric current flows through a solid or liquid with finite conductivity, electric energy is converted to heat through resistive losses in the material. The heat is generated on a microscale as the conduction electrons transfer energy to the conductor's atoms by way of collisions. When an electrical current, I, flows along a conductor, a heat $\dot{Q}J$ is generated within it, by virtue of the Joule effect
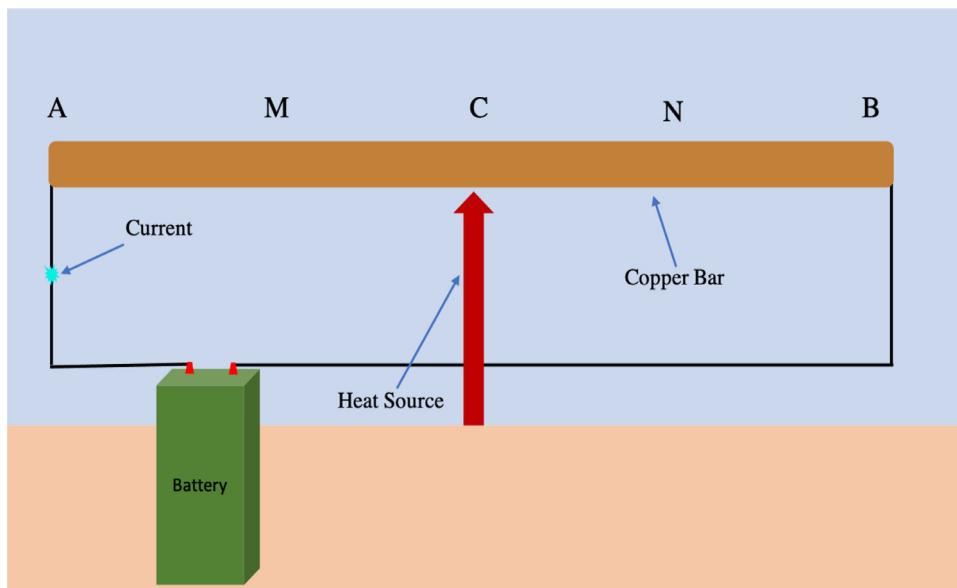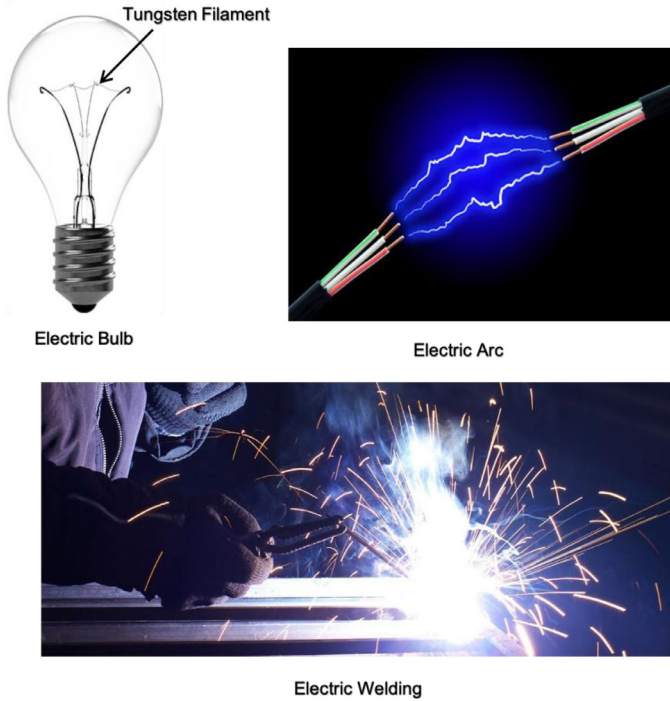

Fig. 3. Thomson Effect Demonstration [34].

Fig. 4. Applications of Joule's Heating Effect [37].

$$\dot{Q}J = \ I^2R \tag{2}$$

where R represents the electrical resistance [36].

Electric irons, heaters and toasters are some of the home appliances that utilise the heating effect of current. Electric fuses and electric furnaces are also applications of Joule's heating effect.

The electric lamp consists of a tungsten filament mounted inside a glass bulb and heated to incandescence by current. Electric discharge lamps, electric welding and electric arcs also utilise the heating effect of current as shown in Fig. 4.

3. TEG materials, design and optimisation

As mentioned above, thermoelectric generators offer a reliable solid-state solution for energy conversion. Devices using advanced thermoelectric materials can become an alternative to traditional power generation heat engines, most notably in lightweight heat recovery systems. The maximum efficiency of the conversion of thermoelectric energy is typically presented in terms of the temperature of each heat reservoir and the thermoelectric Fig. of Merit (*zT*). As increases in *zT* leads to an improvement in thermoelectric efficiency, substantial efforts have been made to introduce and build materials with high *zT* values [39].

3.1. Analysis of thermoelectric material properties

Effective TE products should be possess the following properties:

- High electrical conductivity in order to minimise Joule heating (increase in temperature from resistance to electric current flowing through it).
- Good Seebeck coefficient for maximum conversion of heat to electrical power or electrical power to cooling performance.
- Low thermal conductivity to avoid thermal conduction through the material.

And such three properties are mainly combined into a single metric which quantifies a thermoelectric device's overall output, the "Fig.-of-Merit" or z.

As z has a unit of per degree of temperature, a more convenient dimensionless Fig.-of-Merit may be used as zT, where T (K) is the average functioning temperature. This is a vital parameter which rules the magnitude of the maximum power conversion efficiency for TE devices [40].

In the past, the only material used commercially for thermoelectric modules was Bismuth Telluride (Bi_2Te_3), for which the value of Fig. of Merit for p-type and n-type materials are 1.35 and 0.9, respectively [41]. The poor productivity of n-type Bismuth Telluride-based materials compared to p-type materials severely limiting its effectiveness as a TE unit [42]. However, Bi_2Te_3 and alloys have been used extensively in TE refrigeration applications and with some low-power niche applications, and have a useful temperature range from 180 to 450 K.

PbTe and *SiGe* materials have been used widely in higher-temperature power generation applications, mostly in spacecraft power production, with a reasonable temperature range of 500 to 900 K and 800 to 1300 K, respectively [40]. Investigations have shown that these generally have a Fig. of Merit of about 1.

Fig. 7 shows the graph for the efficiency of the TE module with regard to the temperature differential between the cold and the hot side (the aim is to get as close to the efficiency of the Carnot cycle as possible). For an average Fig. of Merit of 1, the efficiency is around 10% and, in order to increase efficiency further than that, the zT needs to reach a higher value [43].

Nevertheless, in order to compensate for a lack of performance, scientists have sought to develop other approaches in addition to that of increasing zT, such as extending the functional area of materials to work with greater temperature variations and, most notably, developing low-cost materials. Except for the space industry, Bismuth Telluride modules (Bi_2Te_3) were the only materials which were available for industry at a reasonable price. However, the quantity of Bismuth and Telluride within the crust of earth and in the ocean is small [44], which has become another challenge for manufacturers. On the other hand, the space industry has been a big manufacturer of thermoelectric technologies, but their products were mostly utilised for space applications owing to their high expense of development.

Over the past two decades, scientists and companies have been looking hard for an environmentally friendly replacement material that could be produced commercially in large quantities.

Thermoelectric materials can be classified into two categories, namely conventional and new materials.

3.1.1. Conventional TE materials
The conventional thermoelectric materials, which are bulk semiconductor alloys or chalcogenides, may be categorised into three
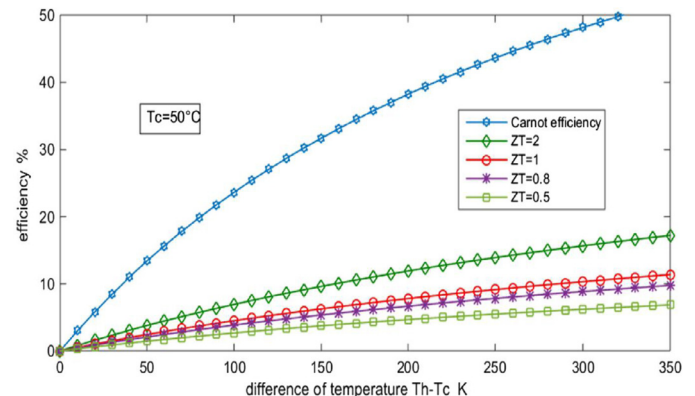

Fig. 7. Typical Values of TE Efficiency for Different Values of zT for Bi_2Te_3 [43].

groups depending on the temperature range at which the capacity is optimum. For instance, for applications of temperature range of less than 150 °C, Bi_2Te_3- based materials, for applications of temperature range of 150 to 500 °C, TAGS [$AgSbTe_2$]1 − x($GeTe$)x] and $SiGe$- based materials at temperatures over 500 °C [45,46]. The temperature spectrum can be expanded by using a mixture of materials distinguished by the temperature levels in the segmented structure [47].

Bi_2Te_3 is well known thermoelectric material and may have a Fig. of merit close to 1 at room temperature. Nonetheless, since these materials are readily oxidised and vaporised, they cannot be used for high temperature applications in the air [48]. Approximately 70% of the commercially available TE modules use Bismuth and Telluride as operational materials [49]. Mamur et al. [50] have analysed the new studies on the development of the Bi_2Te_3 nanostructure by different methods and its characterization by theoretical and analytical approaches. The authors inferred that the Fig. of merit would grow from 0.58 to 1.16 if the materials were formed in a nanostructure shape.

Lead telluride ($PbTe$) is a suitable thermoelectric material for applications involving temperatures of up to 900 K. This material has a high melting point of 1190 K, decent chemical consistency, low vapour pressure and a solid chemical strength [51]. Moreover, its high Fig. of merit, reaching 0.8, enabled it to be used successfully in many NASA space missions. Latest investigations have recorded maximum ZT values of approximately 1.4 for single phase $PbTe$ -based materials and 1.8 for homogeneous $PbTe − PbSe$ materials [52].

References [53,54] include a detailed survey of $PbTe$ Research and Development and its associated compounds, alloys and composites, as well as $PbTe$-based nanostructured composites. Silicon−Germanium alloys ($Si_{1 − x}Ge_x$) are among the strongest TE materials recorded in high-temperature literature ($T_{hot} > 500°C$). In addition, they are one of the simplest and most non-toxic thermoelectric materials [45]. Delime-Codrin et al. [55] documented a substantial Fig. of merit of 1.88 at 873 K, with nanostructured $Si_{0.55}Ge_{0.35}(P_{0.1}Fe_{0.01})$.

3.1.2. New TE materials

Indicated in Fig. 1, a phonon-glass electron-crystal (PGEC) proposed by Anno et al. [56] which have a complex intermetallic cage structure which gives the material good electronic characteristics simultaneously, it has a low thermal conductivity. In general, two types of comparatively recent materials are known to be PGEC materials, namely clathrates and Skutterudites [57].

As for their desirable electrical transport properties, relatively high Seebeck coefficients and rich element combinations, half-Heusler alloys have received significant attention comparing to other TE materials [58]. Additionally, they perform mechanical strength, good thermal stability at high temperatures and multiform physical properties [59]. Gascoin et al. [60] suggested the Zintl phase as a suitable candidate for thermoelectric materials. They are typically small-bandgap semiconductors with a complex structure. Since then, several studies have been conducted on the use of this category of material and the finest values accomplished for the Fig. of merit varied from 1 to a peak value of 1.5 [61].

Several attempts have been made to achieve high-performance thermoelectric materials for energy transfer systems following the discovery of the first ceramic thermoelectric material [62]. TE oxides, such as $Ca_3Co_4O_9$ ($ZT \sim 1$), are strong performers of TE [63] and are environmentally sustainable and relatively withstand high temperatures [64].

Thermoelectric metal chalcogenide has high electrical properties and poor thermal conductivity, but when advanced nanostructures and band engineering are used the result is an increased Fig. of merit (zT). In addition, chalcogenides are easy to process in various types of structures, thereby giving an excellent platform for thermoelectric efficiency enhancement. The highest Fig. of merit values observed with lead selenide ($PbSe$) ranged from 1.4 to 1.7 at 800−900 K [65]. In the case of T in chalcogenides Sn (Se, Te), the numerical values of Fig. of merit above 2.3 were obtained at 723−973 K for single crystal $SnSe$ [66] and at approximately 1.6 for $SnTe$ -based materials at 923 K [67]. Another advantage is that these products are low-cost and work at high and even medium temperatures. However, their poor mechanical properties and low thermal stability and, in some situations, the occurrence of harmful elements such as Pb restrict their use in actual applications

A great deal of interest has been seen in organic TE materials since the discovery of conductive polymers [68]. They are lightweight, compact and ideal for room temperature applications typically with comparatively easy manufacturing processes compared to other semiconductor-based materials. Polymers are naturally ineffective thermal conductors, making them ideal for use in thermoelectricity, but their low electrical conductivity, Seebeck coefficient and stability have limited their use in thermoelectric applications [69]. However, opposed to inorganic TE materials, organic or polymeric TE materials have numerous advantages, such as a potentially low cost due to the availability of carbon supplies and a comparatively easy synthesising process. In addition, the physical and chemical properties of certain polymers can be susceptible to a reasonably broad variety of modifications in their molecular structures [70].

Graphene (carbon atoms forming a crystalline two-dimensional material) which is another substance, has drawn tremendous attention since its discovery as it has many uncommon thermoelectric and thermal transport properties [71]. A recent research published thermoelectric merit Fig. (zT) up to 1.4 with graphene and C60 clusters synthesised by chemical vapour deposition (CVD) [72]. A further experimental analysis showed three peak zT values of 2.0, 2.7 and 6.1 at 300 K, with a twisted bilayer graphene nanoribbon junction [73].

3.2 TEG performance analysis and expressions

3.2.1. Thermoelectric figure of merit

The Fig. of Merit is dimensionless and in order for TEGs to have a high efficiency, the value of zT should be as high as possible. In the numerator, the quantity ($S^2\sigma$) known as the Power Factor (PF), is a vital element for maximizing the Fig. of Merit zT. The Fig. of Merit can be calculated from Eq. (3 [74,75]:

$$zT = \frac{S^2\sigma T}{K_{total}}$$ (3)

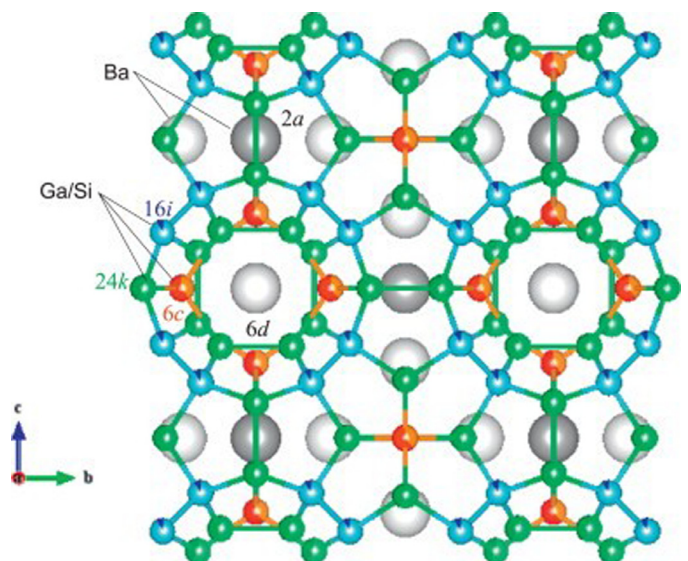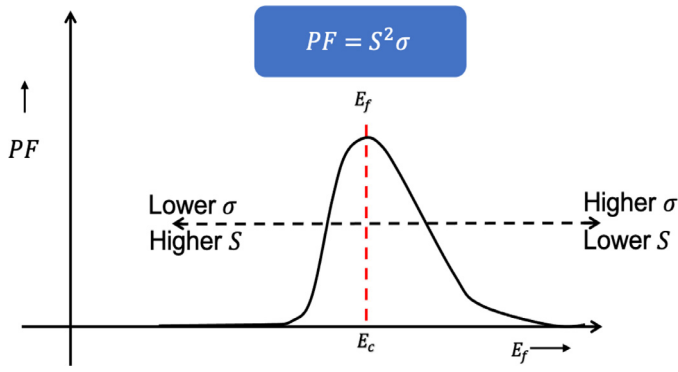**Fig. 8.** Clathrate crystal structure [56].

Fig. 9. Power Factor vs. Fermi level [77].

Fig. 10. Location of Fermi Level for Intrinsic Semiconductors [80].

Fig. 11. Location of Fermi Level for Extrinsic Semiconductors [80].

where S is the Seebeck coefficient, σ is the electrical conductivity, and T is the average temperature, K_{total} is the total thermal conductivity and it is the summation of K_l and K_e which are the thermal conductivity due to the lattice and due to the electrons respectively.

3.2.1.1. Fermi level. The Power Factor (PF) is used as a thermoelectrical performance measure, the electrical conductivity is comparative to the carrier density, and the Seebeck coefficient is in inverse proportion to the carrier density. Hence, Fermi level optimisation is vital for maximising thermoelectric performance.

Ohtani [76] defines the Fermi level in the form of the quantity of electrical equilibrium energy in a solid material. Also, it is believed that the Fermi energy is the energy of the most energetic electron at the absolute zero of temperature (T = 0 K).

The power factor and therefore the Fig. of Merit strongly depend on the position of the Fermi level. The power factor is optimised when the Fermi level is positioned near the bottom of the conduction band (actually, depending on details, a little below the bottom or a little above the bottom, depending on band structure and scattering).

Thus, if the power factor is plotted against the Fermi level as shown in Fig. 9, the peak occurs when the Fermi level is positioned near the bottom of the conduction band. This is due to the different dependences of the electrical conductivity and the Seebeck coefficient on the Fermi level.

To get a high Power Factor, requires doping the semiconductor such that the Fermi level can be placed where it needs to be in order to maximise the parameter. Moreover, high conductivity at low Fermi energy is also necessary, which means that, the conduction band should have a lot of channels so there will be no need to push the Fermi level inside the conduction band which lowers the Seebeck coefficient [78].

In other words, all states with lower energies than E_f are filled and all states above E_f are empty at T = 0 K. Nevertheless, in insulators and semiconductors the Fermi level occurs in the energy gap between the valence and conduction bands.

At T = 0 K, it is often the case that states with energy lower than E_f are filled and those with energy greater than E_f are vacant. But the exact position of E_f in the energy gap is determined by the function of the Fermi distribution as shown in Eq. (4) [79]:

$$f(E) = \frac{1}{1 + \exp\left(\frac{E - E_f}{kT}\right)} \tag{4}$$

That is, E_f is the energy such that the Fermi distribution function $f(E)$ accurately determines the distribution of electrons between the usable states in the valence and conduction bands. E is the electronic charge, k is Boltzmann's constant, and T is the average absolute (Kelvin) temperature of the sample.

For intrinsic semiconductors (the pure form of the semiconductor), E_f is predicted to exist in the centre of the energy gap —
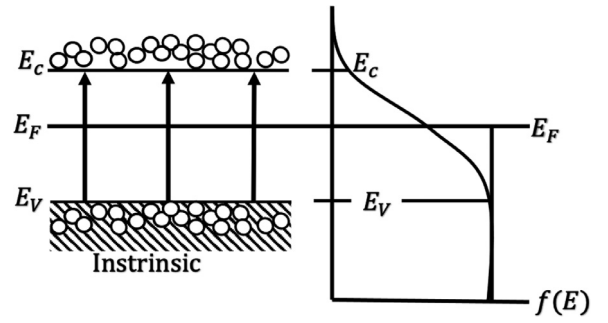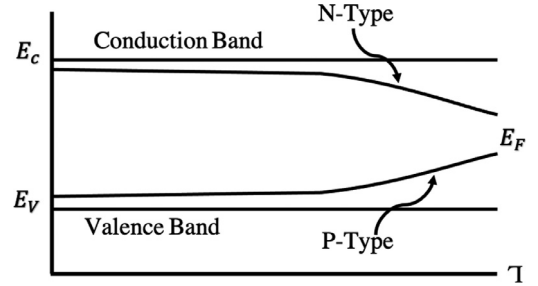
representing an equivalent possibility of electrons in the conduction band and holes in the valence band at a specified temperature (see Fig. 10) [80].

However, in extrinsic semiconductors (i.e. a doped semiconductor in which intentional impurities are added for making it conductive), E_f exists (at low temperatures) either within the conduction band (n-type) or the valence band (p-type) depending on the majority carriers' sign and concentration and the absolute temperature (Fig. 11).

3.2.1.2. Nanotechnology. High zT values have been challenging to obtain owing to the intrinsic relationship between electrical conductivity and thermal conductivity of most materials. High electrical conductivity is required to reduce the temperature resistance (Joule) of the TE unit, whereas low thermal conductivity is required to sustain a stable temperature differential between the hot and the cold side [81].

However, another way to increase the Fig. of Merit is by reducing the total thermal conductivity (K_{total}). To achieve this, scientists have succeeded in artificially structuring materials at the nanoscale and engineering the thermal conductivity of the lattice, reducing it from the value that it would normally have in a bulk material.

For instance, in Fig. 12, this is achieved by adding a large density of grain boundaries and other dispersion centres that effectively diffuse phonons but are not very efficient in scattering electrons. Basically, it is an effort to substantially reduce the thermal conductivity of the lattice while not dramatically impacting the electrical conductivity and this has recently proved to be successful [82].

Fig. 13 demonstrates the history of developments in thermoelectric technology. Initially, there was gradual advancement before 1970 at which point in time a Fig. of Merit 1 was achieved. This was then followed by a period when there was virtually no improvement until the concept of utilising nanostructures to boost thermoelectric efficiency was adopted and the Fig. of Merit dramatically improved. This is because the thermal conductivity of the lattice is designed to lower and lower values [83].

In the near future, the components used in TEGs are nanostructured nanocomposite TE materials, as they can be assembled in a set of various designs for system applications and can be scaled up for industrial applications. Nanocomposites have also demonstrated
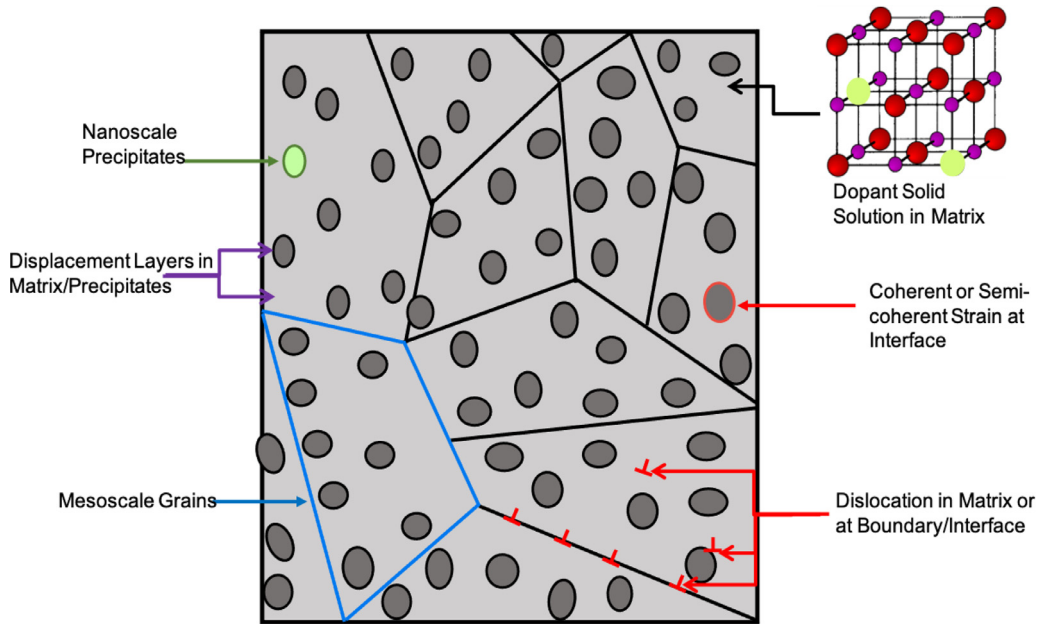
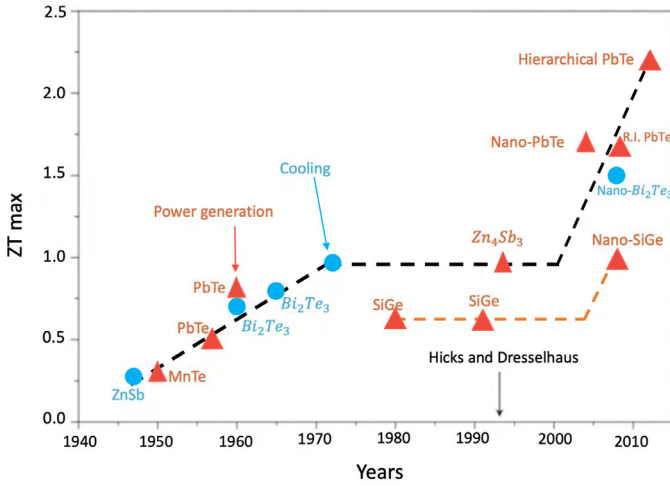**Fig. 12.** Phonon Mean-Free-Path Engineering [77].

Fig. 13. The Value of zT in Time with advancement of Nanotechnology [83].

significant increases in thermoelectric performance over their bulk equivalents, and many can be processed using affordable processing techniques. It must be mentioned that the specifics of nanostructures and the requirements of preparation would have a major influence on the effectiveness of nanocomposite TE materials, and further research in order to gain a deeper understanding is required to enable the rational design and preparation of nanocomposites and to facilitate the widespread adoption of thermoelectric materials [84].

TE nanoscale and nanostructured materials are shown in Table 1.

3.2.2. Efficiency of TEG

The efficiency of a TEG can be defined as the ratio of the electrical energy produced (W_{elec}) to the thermal energy entering the hot face (QH) and it can be approximated by Eq. (5) for optimal electrical charge [85]:

$$\eta_{\text{TEmax}} = \frac{W_{elec}}{QH} = \frac{\Delta T}{T_H} \times \frac{\sqrt{1 + zT} - 1}{(\sqrt{1 + zT}) + \frac{T_c}{T_H}} \tag{5}$$

where zT is typically assessed at the mean temperature of the hot side temperature (T_H) and the cold side temperature (T_c). From the

equation, it is obvious that a rise in zT contributes to an improvement in energy conversion capacity.

Moreover, the maximum power generated by the TEG can be predicted via Eq. (6) [86]:

$$P_{\max}(w) = \frac{\Delta T}{T_H} \times \dot{Q} \times \frac{\sqrt{1 + zT} - 1}{(\sqrt{1 + zT}) + \frac{T_c}{T_H}} \tag{6}$$

where $\dot{Q}$ represents the rate of heat transfer through the TEG (W), which can be described as the ratio of the temperature difference to the TEG thermal resistance as shown in Eq. (7) [87] ($R_{TEG} \circ C/W$):

$$\dot{Q}(w) = \frac{\Delta T}{R_{TEG}} \tag{7}$$

A TEG can produce its maximum power when it operates at half the open circuit voltage and half the short circuit current. An alternative means of deducting a TEG 's potential strength may be written as Eq. (8) [86]:

$$P = VI \rightarrow P_{\max} = \frac{1}{2} V_{\text{Open Circut}} \times \frac{1}{2} I_{\text{Short Circut}} \rightarrow P_{\max} = \frac{1}{4} V_{\text{OC}} \times I_{\text{SC}} \tag{8}$$

4. TEG Case Studies and Applications

Thermoelectricity, in the form of thermoelectric generators, has a strong capacity for waste heat recovery, and has been researched and demonstrated in a variety of experimental and theoretical works. Through the use of a thermoelectric generator, part of the energy that is usually lost during the production operation can be converted into electricity.

The transport sector might be the most desirable sector to use thermoelectric generators to recover lost heat. Until now, there have been few solutions to recycle the excess heat from the engine exhaust gas. The most successful field for energy recovery is the automobile market, where competition for ever-cleaner automobiles is quite dynamic and government-sponsored.

4.1. Automotive

Automotive industrialists are projecting a great deal of interest to thermoelectric generators in order to turn the heat wasted by the

Table 1
Thermoelectric properties, low-dimensional and nanostructured materials [84].

Material systems	Carrier type	ZT	K_l [W/m. K]	T
Skutterudites $CoSb_3$				
$Yb_{0.19}Co_4Sb_{12}$	n	1	–	600 K
$In_{0.25}Co_4Sb_{12}$	n	1.2	2	575 K
$CoSb_{2.75}Sn_{0.05}Te_{0.2}$	n	1.1	2.04	823 K
$Ba_{0.14}In_{0.23}Co_4Sb_{11.84}$	n	1.34	0.74	850 K
$Yb_{0.2}Co_4Sb_{12.3}$	n	1.26	–	800 K
$Yb_{0.3}Co_4Sb_{12.3}$	n	1.3	–	800 K
$Na_{0.48}Co_4Sb_{12.3}$	–	1.25	–	850 K
$Ba_{0.08}La_{0.05}Yb_{0.04}Co_4Sb_{12}$	n	1.7	–	850 K
2D Materials: quantum well or superlattices				
$PbTe/Pb_{1-x}Eu_xTe$	–	2	–	293 K
$PbSeTe/PbTe$	n	2	0.58	293 K
Bi_2Te_3/Sb_2Te_3	p	2.4	0.22	300 K
$Bi_2Te_3/Bi_2Te_{2.83}Se_{0.17}$	n	1.4	0.58	300 K
Bi_2Te_3-based nanocomposites				
$BiSbTe$	p	1.4	–	373 K
$Bi_2Te_{2.75}Se_{0.3}$	n	1.04	–	498 K
$(BiSb)_2Te_3$	p	1.47	–	440 K
$Bi_{0.52}Sb_{1.48}Te_3$	p	1.56	0.26	300 K
Bi_2Te_3	n	1	0.3	450 K
$Bi_{0.4}Sb_{1.6}Te_3$	p	1.5	0.16	293 K
$PbTe$-based nanocomposites				
$AgPb_{18}SbTe_{20}$	n	2.2	–	800 K
$Ag_{0.5}Pb_6Sn_2Sb_{0.2}Te_{10}$	p	1.45	0.43	630 K
$Ag_{0.53}Pb_{18}Sb_{1.2}Te_{20}$	n	1.7	–	700 K
$K_{0.95}Pb_{20}Sb_{1.2}Te_{22}$	n	1.6	0.4	750 K
$Na_{0.95}Pb_{20}SbTe_{22}$	p	1.7	0.74	700 K
$PbTe - PbS 8\%$	n	1.4	–	750 K
$PbTe - Pb - Sb$	n	1.4	0.6	700 K
$PbTe - Si$	n	0.9	–	675 K
$Pb_{9.6}Sb_{0.2}Te_3Se_7$	n	1.2	0.4	650 K
$(Pb_{0.95}Sn_{0.05}Te)_{0.92}(Pb)_{0.08}$	n	1.5	0.4	642 K
$2\% SrTe - containing\ PbTe$	P	1.7	0.45	800 K
$NaPb_{18}BiTe_{20}$	p	1.3	–	670 K
$Ag_{0.8}Pb_{22.5}SbTe_{20}$	n	1.5	0.89	700 K
$SiGe$-based nanocomposites				
$Si_{80}Ge_{20}$	p	0.95	–	1073 K
$Si_{80}Ge_{20}P_2$	n	1.3		1173 K
New thermoelectric materials				
$In_4Se_{3-\delta}$	n	1.48	–	705 K
$In_4Se_{3-x}Cl_{0.03}$	n	1.53	–	698 K
$\beta - Cu_{2-x}Se$	p	1.5	0.4	1000 K
$\beta - Zn_4Sb_3$	p	1.35	–	673 K

exhaust gas produced by the internal combustion (IC) engine into electrical energy [88]. In a motor car, about 25% of the fuel-fired capacity is used for vehicle mobility and operating accessories, while 40% is spent on exhaust gas [89] . On the other hand, the amount of heat generated from the exhaust system is very high and could range from 100 C to 800 C with a thermal output of up to 10 kW depending on the vehicle speed and the fuel category. This significant amount of heat may be viewed as a valuable source of sustainable and adequate energy.

The transfer of emitted heat would also be the key solution for enhancing engine efficiency and supplying additional electronic equipment such as guidance systems, electronic brakes, additional powertrain/body controllers, stability sensors, telematics and accident prevention systems for conventional and hybrid vehicles. This would also reduce atmospheric emissions and energy cost.

4.1.1. Automotive waste heat conversion to electric power

Given the high range of the internal combustion engine, it is essential to use more than one form of thermoelements, which would contribute to a better efficiency of conversion. Segmented thermoelectric materials have also been used in this form of application due

to the broad size of the temperature extracted. LaGrandeur et al. [90] have arranged three phases of segmented TE materials as follows: N- and P-type Bi_2Te_3 for low temperature range ($< 250°C$), $P - TAGS$ and $N - PbTe$ for medium temperature range ($250°C-500°C$) and skutterudite materials ($P - CeFe_3RuSb$) and ($N - CoSb_3$) for high temperature range ($500°C-700°C$). In order to monitor the thickness of TE components, thermal expansion coefficient and to maximise the power efficiency of the module, the authors are designing a new TE arrangement for segmented materials. This current design uses a flat TC solution with segmented TE materials between the heat source and the heat sink. This method promotes the possibility of achieving various regions, thicknesses and coefficients of thermal expansion of expansion of materials. In addition to the segmented TEGs, cascaded TEGs have also been requested for vehicle applications [91].

The independent mechanical structure of this method enables the incompatibility of the segmented arrangement to be avoided. Wilbrecht and Beitelschmidt [92] introduced two phases of cascaded TE materials for railway vehicles. The cascaded TEG was made of Bi_2Te_3 ($220°C$) and $Mg_2SiSn/MnSi$ ($410°C$) and provided 2.5 kW of electrical power.

Two TEG positions were used in the literature of the IC engine: the cooling mechanism (radiator) and the exhaust heat exchanger. The first place was given to Crane et al. [93]. They presented the modelling of the integrated TEG radiator and demonstrated its potential to draw enough power from the cooling system to supply the alternator work.

The generators were mounted between the radiator surface and the fins. The estimated temperature difference between the radiator and the fins system was approximately 80°C. In addition, the engine load influences the heat transfer to the radiator and the output power of the TEG. The unit with the use of Bi_2Te_3-based TEG and low engine loads (25%) was able to produce more than 1 kW of electrical power, which could be self-supplied by the alternator and result in a major increase in fuel efficiency.

The second described position of TEG is on the exhaust heat system. The heat exchanger enables the transition of gaseous working fluid from the catalytic converter to the muffler (Fig. 14). Heat exchangers are presented in two forms: flat and cylindrical. Due to the high temperature generated, the placement of TEGs on the exhaust heat exchanger surface has been analysed [94]. The TE modules are attached to the exhaust device surface in a matrix shape. The heat flowing through the exhaust inlet to the exhaust outlet gives thermal energy to the hot sides of the TEG

4.3. Recovery of Waste Heat in Industries

Industry is an area where heat is always a by-product of the operation. In certain cases, some of this heat is reused for heating networks or converted into electrical energy by steam turbines, Rankine or Stirling engines, but much of the time this heat is emitted into the atmosphere. Various waste heat recycling projects using TEGs have been studied.

A field test of the thermoelectric generation system was began [95] at the carburizing furnace of a factory. Residual carburizing gas containing CO, H2 and N2 has been burnt at the site, this resulted in a burning capacity of 20 kW, which continuously heated up the hot side of the TEG. The TEG consisted of 16 Bi_2Te_3 modules and a heat exchanger that received about 20% of the heat (4 kW). The highest electrical output was about 214 W, which reflects an efficiency of 5%, however the electricity used to cool the cold side of the modules was not included in these results.

Aranguren et al. [96] performed laboratory analyses and mathematical tests of a TEG devoted to the recovery of waste heat from a combustion chamber. In their investigation, they included the energy used by the TEG cooling system and addressed various heat exchangers. They concluded that their prototype had a theoretical output of
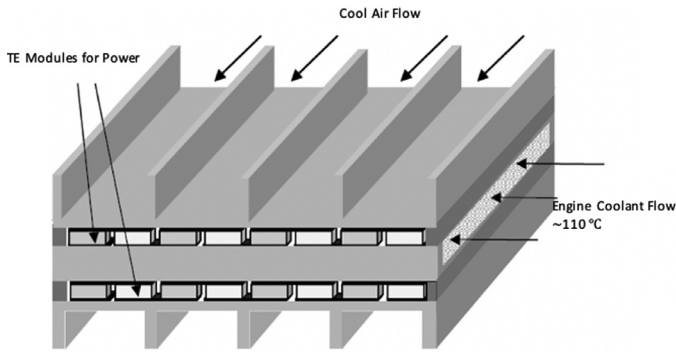
Fig. 14. Schematic demonstration of the TEG locations in the radiator [94].

100 W/m2. This finding was applied to a large industrial chimney on a ceramic tile furnace with a flue gas mass flow of 18,400 Nm3/h and a temperature of 187 C. The forecasted average electrical output was expected to be 136MWh annually [97]. The steel industry produces a lot of waste heat, particularly radiant heat from steel products. TEGs are reliable candidates for the recovery of radiant heat from molten metal.

A company has introduced a 10 kW TEG method (about 4m x 2 m) using radiant heat from continuous casting slabs [98]. The TEG is attached to the grid and consists of 896 TE modules (56 TEG units of 16 Bi_2Te_3 TE) and produces approximately 9 kW when the slab temperature is about 915 C. Cement manufacturing is also an energy consuming industrial process. Luo et al. [99] have researched the feasibility of applying TEGs to Portland cement production. Approximately 10−15% of the energy is dissolved directly into the atmosphere through the outer surface of the rotary turbine.

Due to the permanent movement of the furnace, this kind of waste heat is difficult to recover. For a furnace of 4.80 m in outer diameter and 72 m in length, the gross heat loss without the TEG recovery system is approximately 10,000 kW. A coaxial shell was pictured on the inside of the rotary kiln filled with Bi_2Te_3- $PbTe$ hybrid TE modules.

A theoretical method was developed which estimated that for 20 units with 3480 TE modules (30×30 mm^2) each, the total TE system will generate 210 kW and save 3280 kW because of the insulation shell. The impact of thermoelectric generation is roughly 2%.

These numerous examples and industrial investigations indicate that TEGs have two key opportunities for industrial manufacturing: either in situations where it is challenging to recycle excess heat from traditional systems (radiated heat energy) or in the circumstances where modern materials are able to provide maintenance-free and low-cost electrical power, considering the low performance.

Casi et al. [100] designed a computational model to simulate the performance of a thermoelectric generator that absorbs waste heat from hot fumes. Using the computational model, the optimum design of the thermoelectric generator is acquired. In addition, an experimental investigation of the behaviour of various heat pipes operating as cold side heat exchangers is accomplish, that was done to improve the performance of the whole thermoelectric generator, thermal resistance of less than 0,25 K/W is achieved.

The optimised design of the thermoelectric generator was designed, assembled and tested under real conditions and experimental data was collected. The findings show that 4.6 W of average electrical power is generated during the test cycle with an efficiency of 2.38%. The experimental evidence is used to verify the numerical model. Furthermore, the maximum harvesting capacity of an integrated configuration that takes advantage of the entire pipe is measured using a validated computational model, resulting in 30.8 MWh
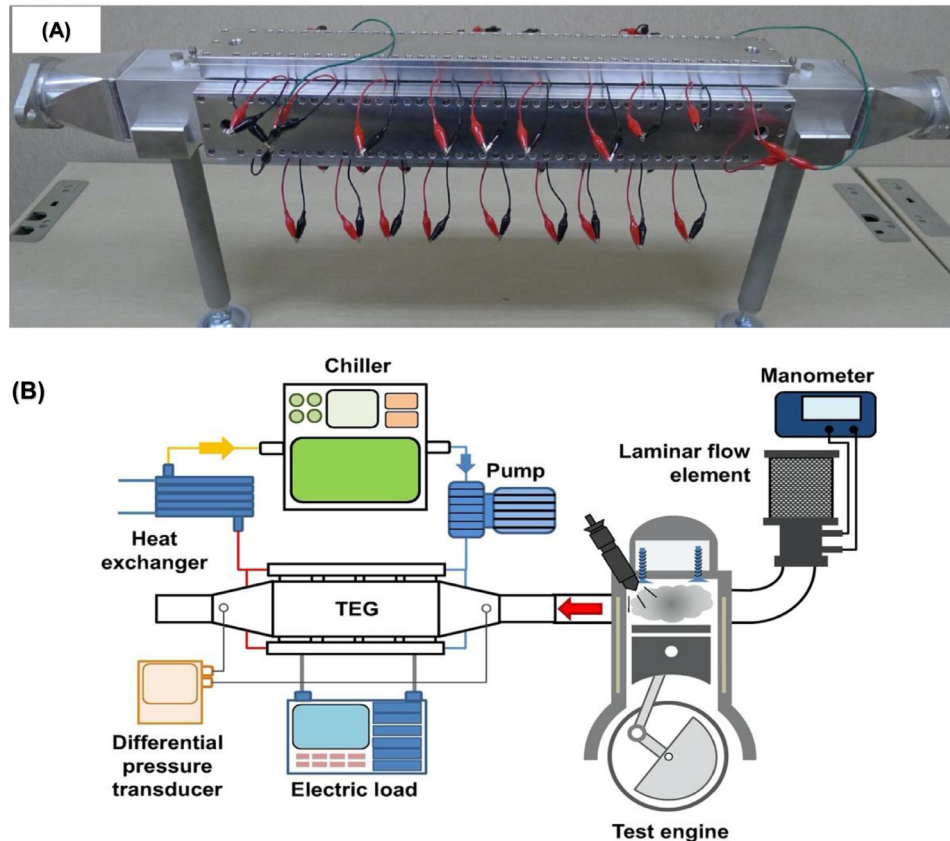

Fig. 15. **(A)** The Used DCTEG when Assembled **(B)** Schematic Diagram of the Experimental Setup [38].

of energy extracted during the sample year, which could satisfy the demand of 8,34 Spanish average households.

Kim et al. [38] proposed the idea of the direct contact thermoelectric generator or DCTEG to boost the feasibility and widen the application areas of thermoelectric generators. One TEM surface is exposed directly to a heat source in the DCTEG, whilst the other surface is in close contact with a coolant flow. The present direct-contact design is useful for system construction, servicing, long-term stability and optimising energy usage in partnership with other energy systems owing to its easy layout and absence of interfaces between the TEMs and their heat sources. To experimentally test the proposed design, a DCTEG was designed by manufacturing modified TEMs and exhaust gas and coolant channels with openings for installing the TEMs.

For the experimental set up, modified TEMs were manufactured to recover waste heat, and, aluminium coolant channels were fabricated with 10 openings and wide flanges around each perforation. To prevent any coolant leakage, a thin layer of sealant was applied around each flange; a rectangular aluminium exhaust gas channel was also fabricated as can be seen in Fig. 15-A.

One TEM surface was exposed directly to the exhaust gas whilst the other TEM surface was exposed to the coolant. Cone-shaped devices were built at both ends of the exhaust gas tube allowing, the DCTEG to be positioned in the centre of an internal combustion engine's tailpipe.

A chiller was used to maintain the coolant at the required temperature. Throughout the experiments a constant coolant flow rate was induced in each coolant channel through the use of a coolant pump and a ball valve assembly. The coolant heated during service was primarily cooled down by a plate-fin heat exchanger before returning to the chiller (see Fig. 15-B).

The TEMs were connected to each other so as to have 10 times the resistance of a single TEM and both ends of the TEM array were attached to the electrical load; the output voltage and the current of the DCTEG being determined as a function of the load resistance.

The trial then started with minimal engine load, and various rotational speed parameters and different brake mean effective pressures (BMEP) until changes in TEG inlet and outlet exhaust gas temperatures and coolant inlet and outlet temperatures were less than ± 0.1 K for a short time (5 minutes continuously). At which points the system was believed to have achieved a steady state.

The average temperature and pressure measurements were then obtained, and the TEG's peak power characteristics were also determined by calculatins of the meassured voltage and current although the resistance to external load varied. The same testing method with specific engine loads and velocities of rotation was repeated (1700 rpm, 2000 rpm, 2300 rpm).

Fig. 16 demonstrates the waste heat recovery performance of the DCTEG in the form of I−V and P−V curves. Part 1 shows the I − V curves of the DCTEG as a function of the engine load at a coolant inlet temperature of 298 K at three different engine speeds. The I − V curves show an almost linear trend, regardless of engine load and rotational speed, implying near-constant electrical resistance during the experiment. Due to the constant resistance of the system, the open circuit voltage V_{oc} and the short circuit current I_{sc} improved linearly with the engine load and rotation speed.

Part 2 displays the P − V curves of the DCTEG as a feature of the engine load and the rotational speed at the inlet temperature of 298 K. At a fixed rotational speed of the engine, the maximum output power increased with the engine load, indicating that the engine cylinder had burned more fuel. The arrows and numbers placed next to the P−V curves indicate the maximum power points and corresponding values. As the engine loads and rotational speeds increase, the TEG output powers increases as well.

5. Performance simulation examples of a TEG

Virtual models and simulations now play a vital role in research and engineering. Digital system analysis is important, particularly when designing and producing a digital product or improving an established device. Numerous software packages are accessible nowadays, scientists and researchers are utilising everything from basic programming languages to various high-level software packages incorporating specialised methods.

Thermal resistance models and numerical simulations are the most common tools for estimating the experimental efficiency of thermoelectric generator systems. Thermal resistance simulations may easily produce analytical outcomes and predict direct preliminary performance analyses of thermoelectric devices [101,102]. Nevertheless, certain simplifications and predictions have to be made in thermal resistance simulations, which may contribute to incorrect outcomes [103].

However, given the long calculation period, numerical approaches are often more appropriate to reliably calculate the distributions of physical parameters that describe the production efficiency of thermoelectric devices. Commercial finite element analysis systems including ANSYS [104] and COMSOL Multiphysics [105], are commonly used to solve numerical equations.

5.1. Autodesk simulation software (ANSYS - computational fluid dynamics)

Autodesk' ANSYS simulation software, part of the Autodesk solution for digital prototyping, provides a range of mechanical simulation tools to help designers, engineers and analysts make decisions earlier in the engineering design process. This has been confirmed by many researchers in their work in their work on TEG, such as studies carried out by L. Montoro et al [106] or by A. Eldesoukey and H. Hassan [107]. With these tools the user can predict the real-world performance of the product helping to save the time and money required to build multiple physical prototypes. The Autodesk simulation software also allows the user to start with mainstream tools and then expand their toolkit to include more advanced simulation such as computational fluid dynamics (CFD).

CFD tools can be used to perform heat transfer and fluid flow simulations in order to study the thermal characteristics of designs and simulate accurate detailed fluid flow behaviour. The setup of CFD simulations is made easier through the use of standard engineering terminology workflow guidance and user-friendly tools and wizards that automate the transfer of simulation results between multiple analyses, letting the user focus on product performance not advanced numerical or simulation methods. Moreover, support for multi CAD environments and finite element modelling tools help manufacturers study initial design intent and accurately predict product performance.

Luoa et al. [108] developed a converging heat exchanger with an attached thermoelectric generator. In order to present comprehensive numerical simulations to evaluate the behaviour of the thermoelectric generator system a fluid-thermoelectric coupled field numerical model was proposed. The computational simulation suggested that the converging thermoelectric generator system generates a higher output power, induces a lower backpressure power loss, and has a more uniform temperature distribution than the conventional structure. The analysis also indicated that at an ambient temperature of 550 K and an air mass flow rate of 60 g/s, the production capacity of the converging thermoelectric generator device is around 5.9% higher than that of the traditional method. In fact, the power boost given by the converging system rises as the air temperature increases and the air mass flow rate decreases. The average output power difference between numerical and experimental tests is
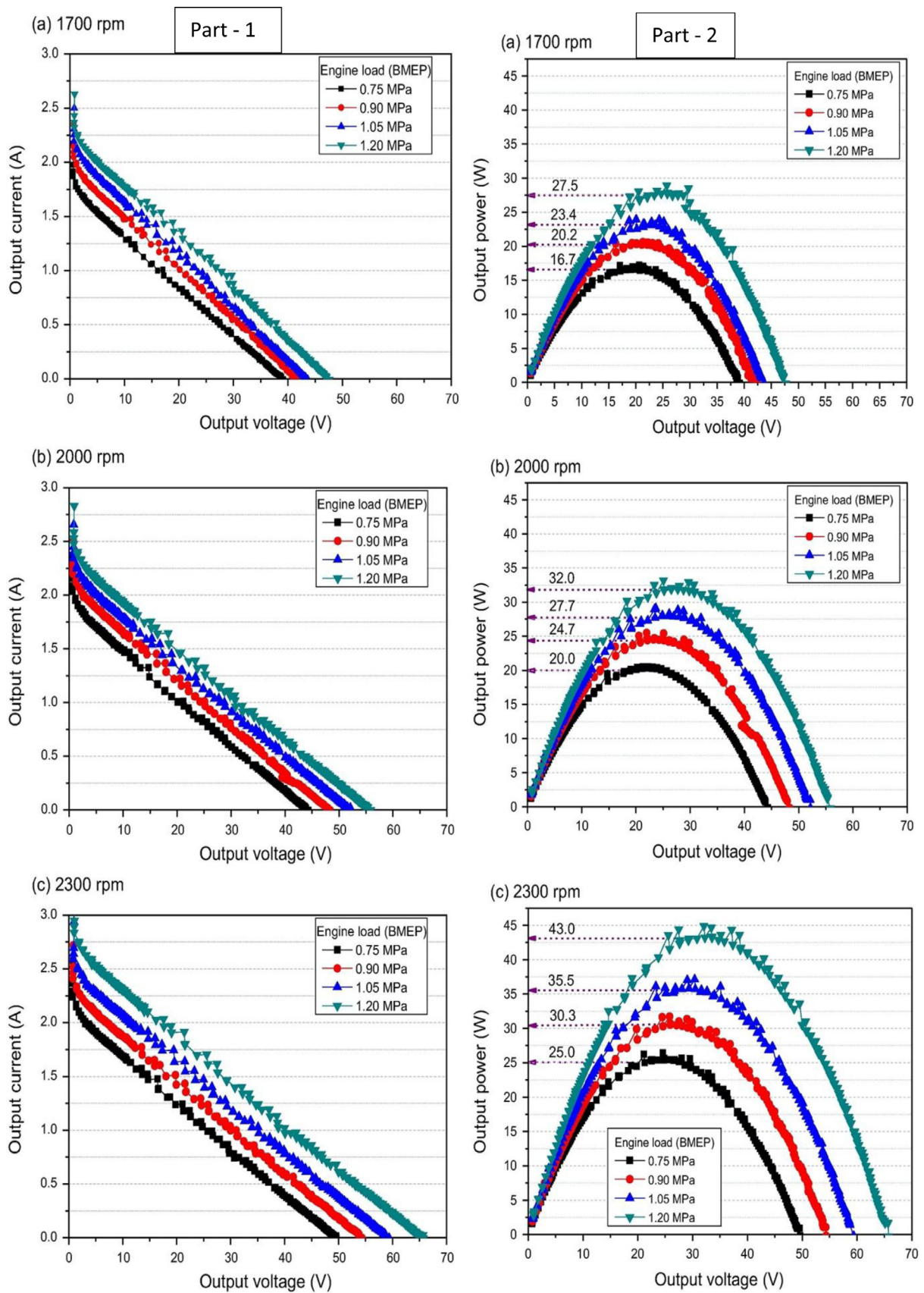
Fig. 16. Part-1: I−V curves for various rotational speeds of (a) 1700 rpm, (b) 2000 rpm, and (c) 2300 rpm. Part-2: P−V curves for various rotational speeds: (a) 1700, (b) 2000, and (c) 2300 rpm [38].
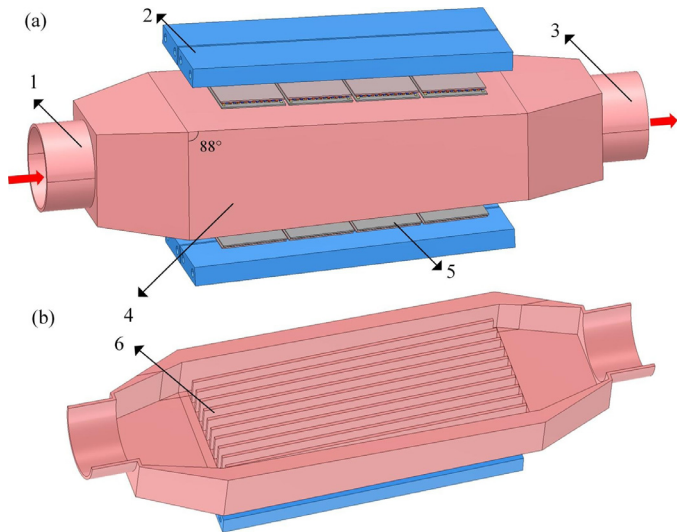
Fig. 17. Schematic diagram of the converging TEG system. (a) The whole body. (b) The cutaway views. 1, Inlet of the HEX. 2, Heat sink. 3, Outlet of the HEX. 4, HEX. 5, TEMs. 6, Internal fin structure of the HEX [108].

Table 2
Material Stress Parameters [113].

Material	Young's Modulus (GPa)	Poisson's ratio	Coefficient of Thermal expansion (1/K)
Copper	119	0.326	1.77×10^{-5}
99.5% Al_2O_3	350	0.3	8.8×10^{-6}
$Sn_{95}Ag_5$	44,5	0.33	2.7×10^{-5}
Bi_2Te_3	-	0.23	-

The objective of this study is to expand the multiphysical fluid-thermoelectric coupled field numerical model from a TEG system containing a single TEM to a TEG system containing multiple TEMs and to subsequently use this novel numerical model to test the efficiency of the proposed TEG convergence system. Finally, the samples of the TEG device are produced and evaluated, and the numerical model is checked in accordance with the experimental findings.

The TEG convergence mechanism contains a HEX, TEMs and heat sinks, as seen in Fig. 17. Both HEX and heat sinks are made of 6063 aluminium alloys. In order to raise the HEX interaction area with hot fluid, several rectangular fins are connected to both hot sides of the HEX. The fins are arranged in the direction of hot fluid downstream, preventing a significant drop in pressure.

only 2.4%, a Fig. low enough to help validate the accuracy of the multiphysics fluid-thermoelectric coupled field numerical model.

5.1.1. Model development 1

Structured optimisation approaches have been extensively used to boost the performance of thermoelectric generator systems, for example improving the conversion efficiency of thermoelectric modules [109] and improving the heat transfer performance of heat exchanger [110]. In view of the high temperature drop that occurs in waste gases during the flow from the inlet to the outlet, this analysis shows a TEG convergence mechanism that mitigates the effect of the temperature drop.

By using the TEG method to recover heat stored in the hot fluid (air in this case), the heat is first absorbed by the heat exchanger (HEX) in the form of conjugate heat transfer, then transferred to the thermoelectric modules (TEM) to produce electricity. The heat is gradually removed by the cooling fluid (water) in the heat sinks.

5.1.2. Experimental results 1

Fig. 18 displays the temperature distribution of the TEG system under the boundary conditions of mass flow rate =60 g/s and temperature of 500 Kelvin. It can be shown that the surface temperature of the HEX is clearly lower than the temperature of the air. The temperature drop from air to HEX is about 60−75 K for the traditional TEG system, while it is only about 50−65 K for the converging TEG system. Approximately, the average temperature gradient of the converging TEG system is 7 K higher than that of the traditional TEG system. That means a higher power output can be produced.

In addition, it can be noted that there is a significant drop in temperature along with a downward flow of air, particularly for the traditional TEG method. The converging nature of the HEX can significantly raise not only the temperature of the hot side but also the uniformity of the temperature. In the case of cold side
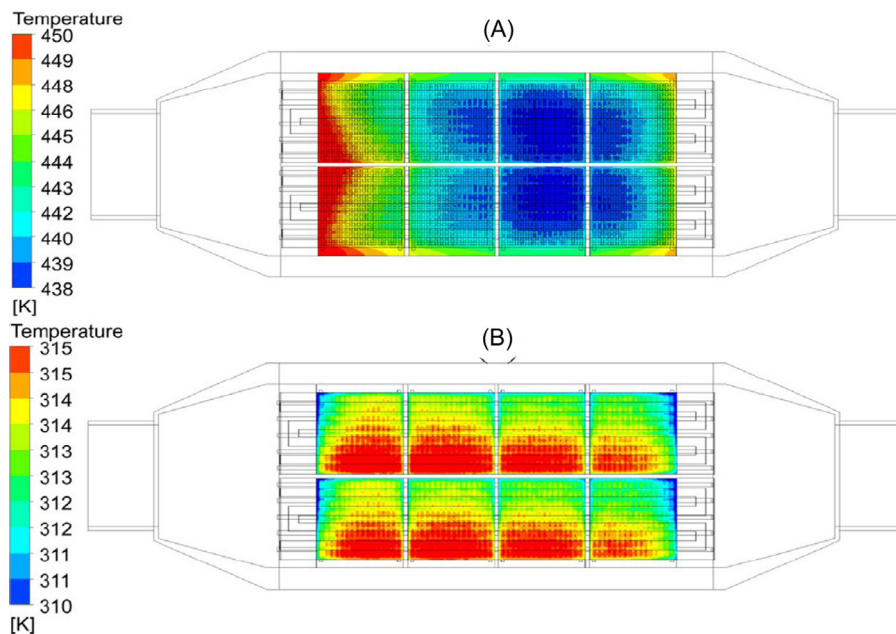

Fig. 18. **(A)** is the hot side and **(B)** is the cold side temperature distributions of TEMs in the converging TEG system, respectively [108].
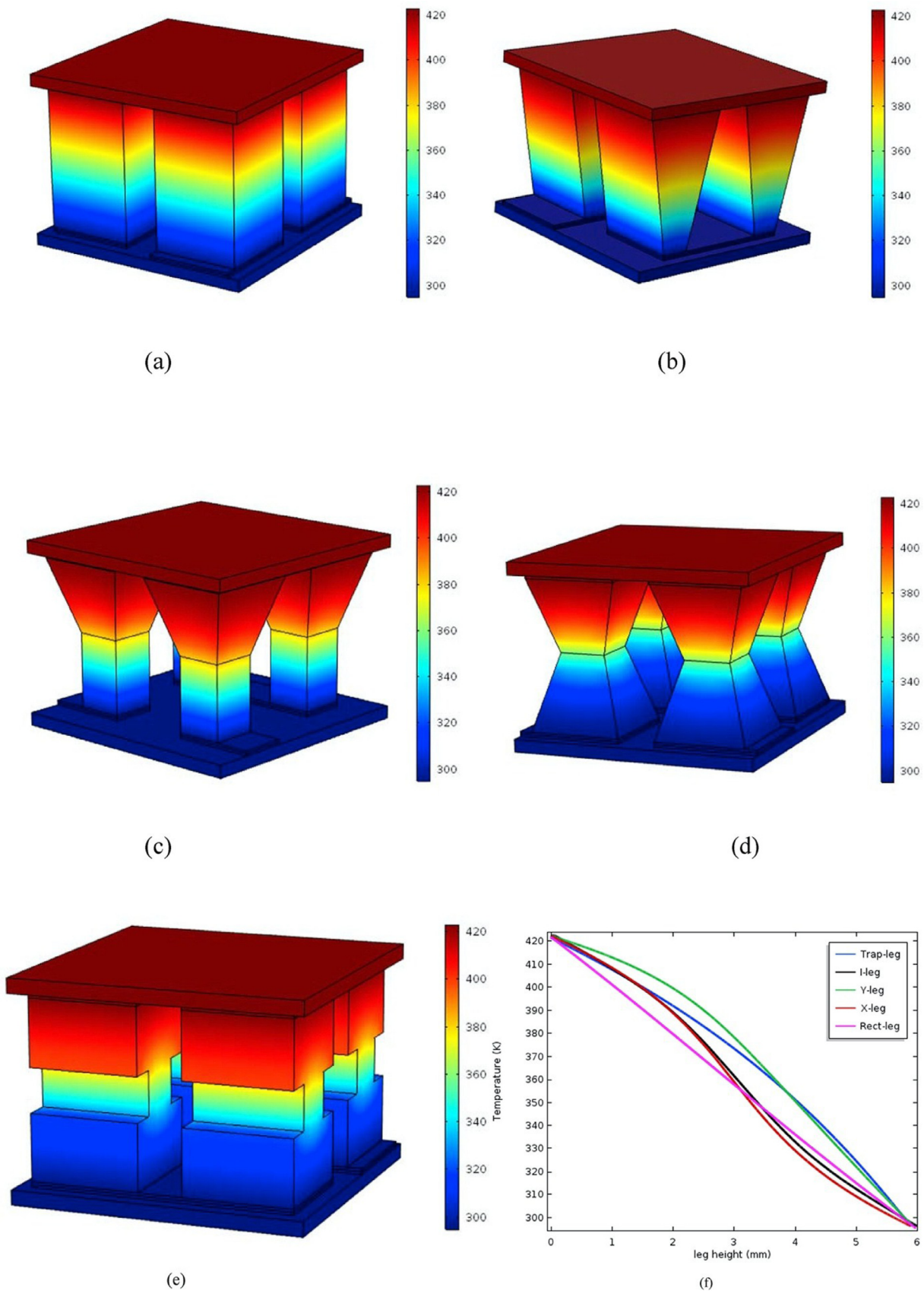
Fig. 19. Temperature distribution of the models. (a). Rectangular leg (b). Trapezoidal leg (c). Y-leg (d). X-leg (e). I-leg (f). Centreline temperature plot [113].

temperature distributions, the temperature of the upper part of each TEM is considerably lower than that of the lower part.

The temperature distributions can be utilised as boundary conditions when computing the electrical output performance of the thermoelectric modules. The converging design of heat exchangers will improve the hot side temperature as well as the temperature uniformity

Overall, the experimental findings were compatible with the theoretical calculations and the maximum error was just about 2.4%; this error arose due to the absence of thermal grease in the numerical simulations. This research therefore offers novel insights into the behaviour of thermoelectric generator systems and introduces a new concept for optimising the exhaust gas channel of the heat exchanger.

5.2. COMSOL multiphysics

COMSOL Multiphysics enables the user to specify the boundary conditions for the model, which in return, leads to achieving reasonably accurate and reliable simulation outcomes. COMSOL is a highly versatile tool that helps the user to apply several physical effects to the prototype. Also, innovative users may create personalised outcomes that are feasible according to their particular circumstances [111].

Adaptability is a benefit of the programme, for example if the consumer wants to add a physical result, or if one of the inputs to the model demands a solution, both may be applied. In fact, all the simulations provided in the COMSOL package can be integrated, for instance electricity is often accompanied by an appropriate thermal effect [112].

Isreallbeagwu [113] used COMSOL Multiphysics to carry out the systematic computational modelling and performance assessment of various types of thermoelectric vector legs with critical analysis under a stable environment. As can be seen from Fig. 15, the study uses different geometries such as rectangular-leg, trapezoidal-leg, Y-leg, I-leg and X-leg, all based on their respective shape structures.

From the study, the variable cross-sectional inclusion was found to influence the performance of the convectional rectangular-leg significantly, such that the X-leg produced around 19.13% higher power density than conventional geometry and was comparatively more effective in all configurations.

In comparison, the X-leg tends to have the maximum entropy density in all design models. This model design faced lower thermal stress than traditional models, while the Y-leg and Trap-leg could have failed structurally before other models. The analysis and simulation results conducted can be used as an important and feasible guide for the design of thermoelectric modules with variable leg configuration of different forms.

5.2.1. Model development 2

The types under consideration are flexible leg TEGs made of copper conductors, $Sn_{95}Ag_5$ solder paste, thermocouples, alumina ceramics and fins. The geometries under analysis include five separate legs, of which 2 are current geometries and the others have been newly developed to increase the temperature differential between the hot and cold junction by changing the cross-section region of the legs. All geometries have the same leg-length of 6 mm and hot junction cross sectional area. The boundary condition for the material stress parameters is shown in Table 2.

5.2.2. Experimental results 2

TEGs with different variable leg geometries were exhaustively modelled with parameters of each leg represented with notation reflecting their geometry. The numerical computations were performed under steady state conditions with the hot and cold ceramic
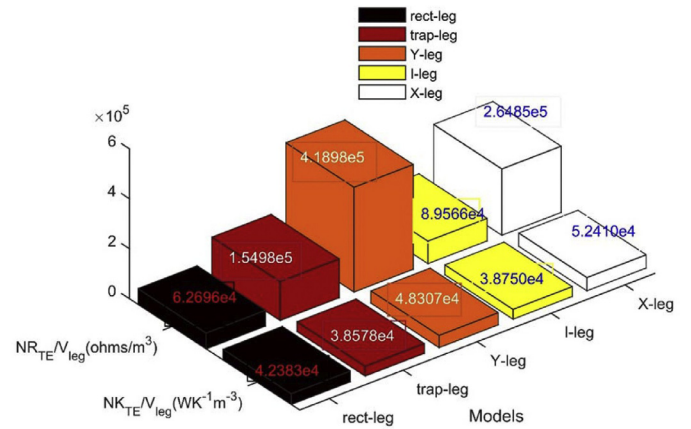

Fig. 20. Total internal resistance and thermal conductance of the models for a unit volume [113].

plates in contact with the junctions held at 423 K and 295 K respectively for all models.

The temperature distributions of the different models are shown in Fig. 19. The solder paste, copper strip, and ceramic plate are combined with the thermoelements. As shown in Fig. 19, the temperature decreases significantly from the hot plate to the base cold plate for all test samples. In addition to ensure closely balanced physical properties, the coefficients of thermal expansion of the n- and p-type materials must be similar in order to prevent the application of stresses under the device's operating conditions.

From the centreline plot in Fig. 19(f) the rectangular-leg indicated a relatively linear profile along the decay path whilst others presented diverse kinds of curved paths; this is due to the variability in their respective cross-sectional areas. The X-leg and the I-leg displayed a similar appearance between the angled curves, with no deviation originating from the hot junction at around 2.7 mm of the TEG leg as calculated. In the same way, the trapezoidal-leg had an arc-type curved profile, while the Y-leg had a curvilinear profile, the temperature decay being very extreme along the linear area, which occurred at around 3 mm from the height of the TEG leg to the cold junction.

The various internal resistance of the legs and the conductivity of the different versions have been calculated and are displayed numerically in Fig. 20 with neglect of touch resistance and copper conductor strip resistance under all operational assumptions described previously. This is vital in order to calculate the internal heat generation.

From Fig. 20, the legs displayed distinctive variations in their respective internal resistance per volume relative to each other. This happens as a consequence of modification in model geometry and variability of cross-section regions. The Y-leg is shown to have the maximum internal resistance value per volume with a value of 4.1898e5 Ohms/m3, which is attributed to the fact that regardless of the height of the leg, it is the same. If an effective cross-sectional area is expected over all legs, the Y-leg would have the smallest effective area because resistance per volume is inversely proportional to the square of the area. Similarly, the rect-leg is the lowest with a value of 6.2696e4 Ohms/m3, while the X-leg and the trap-leg are higher than the I-leg and the X-leg is better than the trap leg with about 41.5 %.

Fan et al. [114] have indicated that for the maximum peak power output of the TEG module there is an optimal ratio between the leg's cross-sectional area and its length.

A very interesting relationship between the heat transferred from the hot medium and the power output of TEG, was presented by Chen et al. [115]. Researchers modeled them simultaneously using CFD models. They discovered that the Reynolds number and the exhaust gas velocity had significant influence on the performance of the thermoelectric modul.

Overall and based on the above examples, it seems that only CFD and COMSOL software are used by researchers. Meanwhile, a literature review indicates that the operation of the TEG module can also be modelled using the TRNSYS software. This program allows the user to analyse the work of the module under both transient and steady-state conditions. Massaguer et al [116,117] have developed and validated a longitudinal TEG model in TRNSYS able to simulate its thermal and electrical dynamics. In their next publication they improved the model by taking into account the power losses generated when the TEG array (electrically interconnected) is exposed to temperature fluctuations.

Lineykin and Ben-yaakov [118] proposed a performance analysis of the TEG modules in the Simulink/Matlab software.

6. Conclusion

In conclusion, this review provides a detailed investigation into thermoelectric generation technology and it begins with an extensive description of their operating theory, forms, utilised components, Fig. of Merit and ways to maximise its enhancement strategies such as various configurations of thermoelectric materials and the styles of utilisation of the device substrates. A key obstacle still remains in the design and development of advanced TE materials with acceptable values of Fig. of Merit (zT) and Power Factor, but various methods to achieve a satisfactory efficiency have been analysed.

The functioning of a thermoelectric module is determined by the thermoelectric properties of the n- and p-type materials from which it is composed. High implementation requires both n- and p-type legs to exhibit comparable Fig.s of Merit, although, it was nonetheless discovered that the rigidity of certain compatible materials also places an obstacle to constructing the next generation TEG models.

Flexible contacts can provide a means of alleviating this problem. Furthermore, over the last few decades, major advancements in materials science and nanotechnology have led to a substantial increase in the dimensionless Fig. of Merit, as shown.

Although for other applications discussed within the article, where, for example, temperatures of heat sources change and materials also undergo quite long temperature cycles. Thermoelectric generators have been found as a viable solution for direct generation of electricity from waste heat in industrial processes. Waste heat recovery in manufacturing involves techniques for storing and reusing heat waste from production processes that can then be used to produce usable energy and reduce total energy consumption.

Waste heat is a big challenge in transportation and industry, TEGs are devices which, despite their low efficiency, can contribute to gaining a few percent in overall efficiency and to reducing the environmental footprint. The key benefits of TEGs are their compactness and low maintenance, however, the cost of TEGs based on commercially available materials is still too high.

The low output of the TE components is therefore obscured by the development of the overall method. Nonetheless, well-designed solutions can solve the low performance problem and offer substantial economic or environmental added benefit. The introduction of new low-cost materials and the start-up of TE modules by manufacturers would enable the mass-market production of combined heat and power systems. The roadmap for the future is to develop TEGs with low-cost materials and with low-cost automated process production.

Declaration of Competing Interest

None.

References

[1] J. WIRFS-BROCK, "INSIDE ENERGY," 2015. [Online]. Available: http://insidee-nergy.org/2015/11/06/lost-in-transmission-how-much-electricity-disappears-between-a-power-plant-and-your-plug/. [Accessed 09 11 2019].

[2] "Virtual Chembook," 2003. [Online]. Available: http://chemistry.elmhurst.edu/vchembook/193sources.html#:~:text=Electricity is produced at a,or nuclear energy produces heat.&text=The spinning turbine interacts with, wires to homes and business. [Accessed 29 08 2020].

[3] eia, 22 https://www.eia.gov/tools/faqs/faq.php?id=105&t=3. [Accessed 13 11 2019].

[4] C. Woodford, "ExplainThisStuff," 08 12 2019. [Online]. Available: https://www.explainthatstuff.com/powerplants.html. [Accessed 29 08 2020].

[5] M.T. Børset, Ø. Wilhelmsen, S. Kjelstrup, O.S. Burheim, Exploring the potential for waste heat recovery during metal casting with thermoelectric generators: On-site experiments and mathematical modeling, Energy (2017) 865–875.

[6] A. E. Risseh, H.-P. Nee, O. Erlandsson and J. Dellrud, "Design of a thermoelectric generator for waste heat recovery application on a drivable heavy duty vehicle," 2017.

[7] Sugiartha, S. Negara, Technical feasibility evaluation on the use of a peltier thermoelectric module to recover automobile exhaust heat, The 2nd International Joint Conference on Science and Technology (IJCST), Bali, Indonesia, 2017.

[8] D. Enescu, Thermoelectric energy harvesting: basic principles and applications, IntechOpen 1 (2019) 1–37, doi: 10.5772/intechopen.83495.

[9] J. Chen, K. Li, C. Liu, M. Li, Y. Lv, L. Jia, S. Jiang, Enhanced efficiency of thermoelectric generator by optimizing mechanical and electrical structures, Energies (2017), doi: 10.3390/en10091329.

[10] D. Luo, R. Wang, W. Yu, W. Zhou, A novel optimization method for thermoelectric module used in waste heat recovery, Energy Convers. Manage. (2020), doi: 10.1016/j.enconman.2020.112645.

[11] D. Kraemer, Q. Jie, K. McEnaney, F. Cao, W. Liu, L. Weinstein, Concentrating solar thermoelectric generators with a peak efficiency of 7.4%, Nature Energy (2016), doi: 10.1038/nenergy.2016.153.

[12] Á.A. Bayod-Rújula, A. Martínez-Gracia, A.D. Amo, M. Cañada, S. Usón, J. Uche, J.A. Tejero, Integration of thermoelectric generators (TEG) in Solar PVT panels, Int. Conf. Renew. Energies Power Qual. 17 (2019).

[13] M. Singh, J. Singh, P.Kuchroo Anshula, H. Bhatia, S. Bhagat, G. Sharma, E. Sidhu, Efficient autonomous solar panel and thermo-electric generator (TEG) integrated hybrid energy harvesting system, IEEE Xplore (2016), doi: 10.1109/PIERS.2016.7734785.

[14] E. Bellos, C. Tzivanidis, Energy and financial analysis of a solar driven thermoelectric generator, J. Cleaner Prod. 264 (2020), doi: 10.1016/j.jclepro.2020.121534.

[15] S.S. Indira, C.A. Vaithilingam, K.-K. Chong, M.Faizal R.Saidur, S. Abubakar, Suriati Paiman, A review on various configurations of hybrid concentrator photovoltaic and thermoelectric generator system, Sol. Energy 201 (2020) 122–148, doi: 10.1016/j.solener.2020.02.090.

[16] L. Shen, X. Pu, Y. Sun, J. Chen, A study on thermoelectric technology application in net zero energy buildings, Energy 113 (2016) 9–24, doi: 10.1016/j.energy.2016.07.038.

[17] D.W. Auckland, R. Shuttleworth, A.C. Luff, B.P. Axcell, M. Rahman, Design of a semiconductor thermoelectric generator for remote subsea wellheads, IET 142 (1995) 65–70, doi: 10.1049/ip-epa:19951707.

[18] H. Ishaq, S. Islam, I. Dincer, B. Yilbas, Development and performance investigation of a biomass gasification based integrated system with thermoelectric generators, J. Cleaner Prod. (2020), doi: 10.1016/j.jclepro.2020.120625.

[19] Y. Sargolzaeiaval, V.P. Ramesh, T. V.Neumann, V. Misra, D. Vashaee, M. D.Dickey, M. C.Öztürka, Flexible thermoelectric generators for body heat harvesting – enhanced device performance using high thermal conductivity elastomer encapsulation on liquid metal interconnects, Appl. Energy (2020), doi: 10.1016/j.apenergy.2019.114370.

[20] M. Hyland, H. Hunter, J. Liu, E. Veety, D. Vashaee, Wearable thermoelectric generators for human body heat harvesting, Appl. Energy (2016) 518–524, doi: 10.1016/j.apenergy.2016.08.150.

[21] B. Aravind, B. Khandelwal, P. Ramakrishn, S. Kumar, Towards the development of a high power density, high efficiency, micro power generator, Appl. Energy (2020), doi: 10.1016/j.apenergy.2019.114386.

[22] Alferd, "Applied Thermoelectric Solutions," [Online]. Available: https://thermoelectricsolutions.com/how-thermoelectric-generators-work/. [Accessed 02 08 2020].

[23] H. Jouhara, N. Khordehgah, S. Almahmoud, B. Delpech, A. Chauhan, S.A. Tassou, Waste heat recovery technologies and applications, Sience Direct 6 (2018) 268–289, doi: 10.1016/j.tsep.2018.04.017.

[24] M. Brain, Electronics, 2018 [Online]. Available: https://electronics.howstuffworks.com/diode.htm .

[25] A. Augustyn, "BRITANNICA," 2018. [Online]. Available: https://www.britannica.com/biography/Thomas-Johann-Seebeck. [Accessed 25 10 2019].

[26] D. Stewart, "Famous Scientists," 2016. [Online]. Available: https://www.famousscientists.org/alessandro-volta/. [Accessed 11 2019].

[27] O. Ostroverkhova, Handbook of Organic Materials for Electronic and Photonic Devices, 2nd Ed., Woodhead Publishing, 2019 ed..

[28] M. Naito, T. Yokoyama, Nanoparticle Technology Handbook, 3rd Ed., 2018 ed..

[29] Buschow, K. Jürgen, Encyclopedia of Materials: Science and Technology, 2001.

[30] S. Memon, K.N. Tahir, Experimental and analytical simulation analyses on the electrical performance of thermoelectric generator modules for direct and concentrated quartz-halogen heat harvesting, MDPI (2018), doi: 10.3390/en11123315.

[31] A. Chen, P.K. Wright, Medical applications of thermoelectrics, CRC (2018), doi: 10.1201/b11892-30.

[32] Jamaloei, B. Yadali, The Joule−Thomson effect in petroleum fields: i. well testing, multilateral/slanted wells, hydrate formation, and drilling/completion/production operations, Energy Sources 37 (2) (2015), doi: 10.1080/15567036.2010.551258.

[33] M. Huijben, P. Brinks, Epitaxial Growth of Complex Metal Oxides, Woodhead Publishing, 2015.

[34] "Phsycis for Student," 31 1 2017. [Online]. Available: https://www.youtube.com/watch?v=-VkNtYgb3PQ&t=71s. [Accessed 25 07 2020].

[35] Y. Demirel, Nonequilibrium Thermodynamics, 2nd Ed., 2007 ed..

[36] J. Meseguer, I. Pérez-Grande, A. Sanz-Andrés, Spacecraft Thermal Control, Elsevier, 2012.

[37] Sandhya, "Physics in day to day life," 10 2019. [Online]. Available: http://physicsindaytodaylife.blogspot.com/2012/10/heating-effects-of-electric-current.html. [Accessed 27 07 2020].

[38] T.y. Kim, A. Nagash, G. Cho, Direct contact thermoelectric generator (DCTEG): a concept for removing the contact resistance between thermoelectric modules and heat source, Energy Convers. Manage. (2017) 20–27, doi: 10.1016/j.enconman.2017.03.041.

[39] C.C. Wang, C.I. Hung, W.H. Chen, Design of heat sink for improving the performance of thermoelectric generator using two-stage optimization, Energy 39 (1) (2012) 236–245, doi: 10.1016/j.energy.2012.01.025.

[40] Terry Hendricks, Choate, Engineering scoping study of thermoelectric generator systems for industrial waste heat recovery, U.S. Department of Energy Office of Scientific and Technical Information, 2006.

[41] Y. Lan, A.J. Minnich, G. Chen, Z. Ren, Enhancement of thermoelectric fig.-of-merit by a bulk nanostructuring approach, Adv. Funct. Mater. (2010), doi: 10.1002/adfm.200901512.

[42] M.-K. Han, Y. Jin, D.-H. Lee, S.-J. Kim, Thermoelectric properties of Bi2Te3: CuI and the effect of its doping with Pb atoms, Materials (2017), doi: 10.3390/ma10111235.

[43] D. Champier, Thermoelectric generators: a review of applications, Sience Direct (2017) 167–169, doi: 10.1016/j.enconman.2017.02.070.

[44] B. Gordon, B. Haxel, J.B. Hedrick and G.J. Orris, "USGS Sience for Changing World - Fact Sheet 087-02," 2002. [Online]. Available: https://pubs.usgs.gov/fs/2002/fs087-02/. [Accessed 28 1 2019]

[45] K. Romanjek, S. Vesin, L. Aixala, T. Baffie, G. Bernard-Granger, J. Dufourcq, High-performance silicon−germanium-based thermoelectric modules for gas exhaust energy scavenging, J. Electron. Mater. (2015), doi: 10.1007/s11664-015-3761-1.

[46] M.A. Zoui, S. Bentouba, J.G. Stocholm, M. Bourouis, A review on thermoelectric generators: progress and applications, MDPA (2020), doi: 10.3390/en13143606.

[47] N.M. Yatim, N.Z.I.M. Sallehin, S. Suhaimi, M.A. Hashim, A Review of ZT Measurement for Bulk Thermoelectric Material, AIP Publishing, NY, USA, 2018.

[48] S. Liu, J. Wang, J. Jia, X. Hu, S. Liu, Synthesis and thermoelectric performance of Li-doped NiO ceramics, Ceramic Int. 38 (6) (2012), doi: 10.1016/j.ceramint.2012.02.099.

[49] M.K. Rad, A. Rezania, M. Omid, A. Rajabipour, L. Rosendahl, Study on material properties effect for maximization of thermoelectric power generation, Renewable Energy 138 (2019) 236–242, doi: 10.1016/j.renene.2019.01.104.

[50] H. Mamur, M. Bhuiyan, F. Korkmaz, M. Nil, A review on bismuth telluride (Bi2Te3) nanostructure for thermoelectric applications, Renewable Sustainable Energy Rev. 82 (2018) 4159–4169, doi: 10.1016/j.rser.2017.10.112.

[51] Z.H. Dughaish, Lead telluride as a thermoelectric material for thermoelectric power generation, Physica B 322 (2002) 205–223, doi: 10.1016/S0921-4526(02)01187-0.

[52] A.D. LaLonde, Y. Pei, H. Wang, G. Snyder, Lead telluride alloy thermoelectrics, Mater. Today 14 (2011) 526–532, doi: 10.1016/S1369-702 1(11)70278-4 .

[53] C. Gayner, K.K. Kar, Recent advances in thermoelectric materials, Prog. Mater Sci. 83 (2016) 330–382, doi: 10.1016/j.pmatsci.2016.07.002.

[54] J.R. Sootsman, D.Y. Chung, M.G. Kanatzidis, New and old concepts in thermoelectric materials, Angew. Chem. Int. Ed. Engl. (2009), doi: 10.1002/anie.200900598.

[55] K. Delime-Codrin, M. Omprakash, S. Ghodke, R. Sobota, M. Adachi, M. Kiyama, T. Matsuura, Y. Yamamoto, M. Matsunami, T. Takeuchi, LETTER Large Fig. of merit ZT = 1.88 at 873 K achieved with nanostructured Si0.55Ge0.35 (P0.10Fe0.01), Appl. Phys. Express 12 (2019), doi: 10.7567/1882-0786/AB08B7.

[56] H. Anno, H. Yamada, T. Nakabayashi, M. Hokazono, R. Shirataki, Gallium composition dependence of crystallographic and thermoelectric properties in polycrystalline type-I Ba8GaxSi46−x (nominal x=14−18) clathrates prepared by combining arc melting and spark plasma sintering methods, J. Solid State Chem. 193 (2012) 94–104, doi: 10.1016/j.jssc.2012.03.069.

[57] B.B . Iversen, A.E.C. Palmqvist, D.E. Cox, G.S. Nolas, G.D. Stucky, N.P. Blake, H. Metiua, Why are clathrates good candidates for thermoelectric materials? J. Solid State Chem. 149 (2000) 455–458, doi: 10.1006/jssc.1999.8534.

[58] M. Zou, Jing-Feng Li, T. Kita, Thermoelectric properties of fine-grained FeVSb half-Heusler alloys tuned to p-type by substituting vanadium with titanium, J. Solid State Chem. 198 (2013) 125–130, doi: 10.1016/j.jssc.2012.09.043.

[59] J. Yu, K. Xia, X. Zhao, T. Zhu, High performance p-type half-Heusler thermoelectric materials, Appl. Phys. (2018), doi: 10.1088/1361-6463/aaaa58.

[60] F. Gascoin, S. Ottensmann, D. Stark, S. Haïle, G. Snyder, Zintl phases as thermoelectric materials: tuned transport properties of the compounds Cax-Yb1−xZn2Sb2, Adv. Funct. Mater. (2005), doi: 10.1002/adfm.200500043.

[61] J. Shuai, J. Mao, S. Song, Q. Zhang, G. Chend, Z. Ren, Recent progress and future challenges on thermoelectric Zintl materials, Mater. Today Phys. 1 (2017) 74–95, doi: 10.1016/j.mtphys.2017.06.003.

[62] N.M. Ferreira, Sh. Rasekh, F.M. Costa, M.A. Madre, A. Sotelo, J.C. Diez, M.A. Torres, New method to improve the grain alignment and performance of thermoelectric ceramics, Mater. Lett. 83 (2012) 144–147, doi: 10.1016/j.matlet.2012.05.131.

[63] H. Ohta, K. Sugiura, K. Koumoto, Recent progress in oxide thermoelectric materials: p-Type Ca3Co4O9 and n-Type SrTiO3, ACS (2008), doi: 10.1021/ic800644x.

[64] Y.F. Wang, K.H. Lee, H. Ohta, K. Koumoto, Fabrication and thermoelectric properties of heavily rare-earth metal-doped SrO(SrTiO3)n (n = 1, 2) ceramics, Ceram. Int. 34 (2008) 849–852, doi: 10.1016/j.ceramint.2007.09.034.

[65] C. Gayner, C. K.K.Kar, W. Kim, Recent progress and futuristic development of PbSe thermoelectric materials and devices, Mater. Today Energy 9 (2018) 359–376, doi: 10.1016/j.mtener.2018.06.010.

[66] L.-D. Zhao, C. Chang, G. Tan, M.G. Kanatzidis, SnSe: a remarkable new thermoelectric material, Energy Environ. Sci. (2016), doi: 10.1039/C6EE01755J.

[67] S. Li, X. Li, Z. Ren, Q. Zhang, Recent progress towards high performance of tin chalcogenide thermoelectric materials, J. Mater. Chem. A (2018), doi: 10.1039/C7TA09941J.

[68] T.-C. Tsai, H.-C. Chang, C.-H. Chen, W.-T. Whang, Widely variable Seebeck coefficient and enhanced thermoelectric power of PEDOT:PSS films by blending thermal decomposable ammonium formate, Org. Electron. 12 (2011) 2159–2164, doi: 10.1016/j.orgel.2011.09.004.

[69] Y. Choi, Y. Kim, S.-G. Park, Y.-G. Kim, B.J. Sung, S.-Y. Jang, W. Kima, Effect of the carbon nanotube type on the thermoelectric properties of CNT/Nafion nanocomposites, Org. Electron. 12 (2011) 2120–2125, doi: 10.1016/j.orgel.2011.08.025.

[70] R. Yue, J. Xu, Poly(3,4-ethylenedioxythiophene) as promising organic thermoelectric materials: A mini-review, Synth. Met. 162 (2012) 912–917, doi: 10.1016/j.synthmet.2012.04.005.

[71] W. Duan, J. Liu, C. Zhang, Z. Ma, The magneto-thermoelectric effect of graphene with intra-valley scattering, Chin. Phys. B (2018), doi: 10.1088/1674-1056/27/9/097204.

[72] D. Olaya, C.-C. Tseng, W.-H. Chang, W.-P. Hsieh, L.-J. Li, Z.-Y. Juang, Y. Hernández, Cross-plane thermoelectric Fig. of merit in graphene - C60 heterostructures at room temperature, FlatChem 14 (2019), doi: 10.1016/j.flatc.2019.100089.

[73] S. Deng, X. Cai, Y. Zhang, L. Li, Enhanced thermoelectric performance of twisted bilayer graphene nanoribbons junction, Carbon 145 (2019) 622–628, doi: 10.1016/j.carbon.2019.01.089.

[74] R.V. Ramanujan, K. Deepak, M.S. Pattanaik, Fig. of merit and improved performance of a hybrid thermomagnetic oscillator, Appl. Energy (2019), doi: 10.1016/j.apenergy.2019.113917.

[75] S. Twaha, J. Zhu, Y. Yan, B. Li, A comprehensive review of thermoelectric technology: materials, applications, modelling and performance improvement, Renewable Sustainable Energy Rev. 65 (2016) 698–726, doi: 10.1016/j.rser.2016.07.034.

[76] B. Ohtani, Advances in Inorganic Chemistry, 2011.

[77] M. Lundtrom, "Nano HUB," Purdue University, 02 10 2019. [Online]. Available: https://nanohub.org/groups/mark_lundstrom/. [Accessed 25 06 2020].

[78] V. Janardhanam, Hyung-Joong Yunb, I. Jyothia, Shim-Hoon Yuka, Sung-Nam Leec, Fermi-level depinning in metal/Ge interface using oxygen plasma treatment, Appl. Surf. Sci. 463 (2019) 91–95, doi: 10.1016/j.apsusc.2018.08.187.

[79] "Location of the Fermi Level by Thermoelectric Power Measurements," California, 2015.

[80] "Circuit Glob," 2017 . [Online]. Available: https://circuitglobe.com/intrinsic-semiconductor-and-extrinsic-semiconductor.html. [Accessed 02 07 2020].

[81] D. Wee, Analysis of thermoelectric energy conversion efficiency with linear and nonlinear temperature dependence in material properties, Energy Convers. Manage. (2011), doi: 10.1016/j.enconman.2011.07.004.

[82] Zhi-Gang Chen, Nanostructured thermoelectric materials: current research and future challenge, Prog. Natural Sci. 22 (2012) 535–549, doi: 10.1016/j.pnsc.2012.11.011.

[83] X.W. Wang, H. Lee, Y.C. Lan, G.H. Zhu, G. Joshi, D.Z. Wang, J. Yang, A.J. Muto, M.Y. Tang, J. Klatsky, S. Song, M.S. Dresselhaus, G. Chen, Z.F. Ren, Enhanced thermoelectric figure of merit in nanostructured n-type silicon germanium bulk alloy, Appl. Phys. Lett. (2008), doi: 10.1063/1.3027060.

[84] Z.-G. Chen, G. Han, L. Yang, L. Cheng, J. Zou, Nanostructured thermoelectric materials: Current research and future challenge, Prog. Nat. Sci. (2012), doi: 10.1016/j.pnsc.2012.11.011.

[85] E. Massaguer, A. Massaguer, L. Montoro, J. Gonzalez, Development and validation of a new TRNSYS type for the simulation of thermoelectric generators, Appl. Energy (2014), doi: 10.1016/j.apenergy.2014.08.010.

[86] B. Orr, J. Taglieri, L. Ding, A. Akbarzadeh, Validating an alternative method to predict thermoelectric generator performance, Energy Convers. Manage. (2016), doi: 10.1016/j.enconman.2016.02.074.

[87] J. Wanga, Experimental study on the influence of Peltier effect on the output performance of thermoelectric generator and deviation of maximum power point, Energy Convers. Manage. (2019), doi: 10.1016/j.enconman.2019.112074.

[88] B. Orr, A. Akbarzadeh, P. Lappas, An exhaust heat recovery system utilising thermoelectric generators and heat pipes, Appl. Therm. Eng. 126 (2017) 1185–1190, doi: 10.1016/j.applthermaleng.2016.11.019.

[89] Z.B. Tang, Y.D. Deng, C.Q. Su, W.W. Shuai, C.J. Xie, A research on thermoelectric generator's electrical performance under temperature mismatch conditions for automotive waste heat recovery system, Case Stud. Therm. Eng. 5 (2015) 143–150, doi: 10.1016/j.csite.2015.03.006.

[90] J. LaGrandeur, D. Crane, S. Hung, B. Mazar, A. Eder, Automotive waste heat conversion to electric power using skutterudite, TAGS, PbTe and BiTe, 25th International Conference on Thermoelectrics, 2006, doi: 10.1109/ICT.2006.331220.

[91] A. Krzywaniak, J. Proficz, P. Czarnul, Analyzing energy/performance trade-offs with power capping for parallel applications on modern multi and many core processors, Federated Conference on Computer Science and Information Systems (FedCSIS), 2018.

[92] S. Wilbrecht, M. Beitelschmidt, The potential of a cascaded TEG system for waste heat usage in railway vehicles, J. Electron. Mater. 47 (2018) 3358–3369, doi: 10.1007/s11664-018-6094-z.

[93] D. Crane, G. Jackson, D. Holloway, Towards optimization of automotive waste heat recovery using thermoelectrics, SAE Int. (2001), doi: 10.4271/2001-01-1021.

[94] C. Liu, X. Pan, X. Zheng, Y. Yan, W. Li, An experimental study of a novel prototype for two-stage thermoelectric generator from vehicle exhaust, J. Energy Inst. 89 (2016) 271–281, doi: 10.1016/j.joei.2015.01.019.

[95] H. Kaibe, K. Makino, T. Kajihara, S. Fujimoto, H. Hachiuma, Thermoelectric generating system attached to a carburizing furnace at Komatsu Ltd, AIP Conf. Proc, 2012, doi: 10.1063/1.4731609.

[96] P. Aranguren, D. Astrain, M.G. Pérez, Computational and experimental study of a complete heat dissipation system using water as heat carrier placed on a thermoelectric generator, Energy 74 (2014) 346–358, doi: 10.1016/j.energy.2014.06.094.

[97] D. Champier, Thermoelectric generators: a review of applications, Energy Conversat. Manag. 140 (2017) 167–181, doi: 10.1016/j.enconman.2017.02.070.

[98] T. Kuroki, Research and development for thermoelectric generation technology using waste heat from steelmaking process, J. Electron. Mater 44 (2015) 2151–2156, doi: 10.1007/s11664-015-3722-8.

[99] Q. Luo, A thermoelectric waste-heat-recovery system for portland cement rotary kilns, J. Electron. Mater. 44 (2015) 1750–1762, doi: 10.1007/s11664-014-3543-1.

[100] Á. Casi, M. Araiz, L. Catalán, D. Astrain, Thermoelectric heat recovery in a real industry: from laboratory optimization to reality, Appl. Thermal Energy (2020), doi: 10.1016/j.applthermaleng.2020.116275.

[101] S. Lan, Z. Yang, R. Chen, R. Stobart, A dynamic model for thermoelectric generator applied to vehicle waste heat recovery, Energy (2018), doi: 10.1016/j.energy.2013.01.040.

[102] S. Vale, L. Heber, PJ. Coelho, C.M. Silva, Parametric study of a thermoelectric generator system for exhaust gas energy recovery in diesel road freight transportation, Energy Convers. Manage. (2017), doi: 10.1016/j.enconman.2016.11.064.

[103] M. J-H, Z. X-X and W. X-D., Characteristics analysis and parametric study of a thermoelectric generator by considering variable material properties and heat losses, Int. J. Heat Mass Transfer (2015), doi: 10.1016/j.ijheatmasstransfer.2014.09.023.

[104] C. W-H, L. C-Y and H. C-I, A numerical study on the performance of miniature thermoelectric cooler affected by Thomson effect, Appl. Energy (2012), doi: 10.1016/j.apenergy.2011.08.022.

[105] D. Ebling, M. Jaegle, M. Bartel, A. Jacquot, H. Böttner, Multiphysics simulation of thermoelectric systems for comparison with experimental device performance, J. Electron. Mater. (2009), doi: 10.1007/s11664-009-0825-0.

[106] L. Montoro, A. Massaguer, E. Massaguer, M. Comamala, R. Fernández, A. Deltell, Utilization of residual heat in Diesel engines, CFD simulation of a thermoelectric generator, International Conference on Renewable Energies and Power Quality, 2017.

[107] A. Eldesoukey, H. Hassan, 3D model of thermoelectric generator (TEG) case study: effect of flow regime on the TEG performance, Energy Convers. Manage. 180 (2019) 231–239, doi: 10.1016/j.enconman.2018.10.104.

[108] D. Luoa, R. Wanga, W. Yub, W. Zhoua, A numerical study on the performance of a converging thermoelectric generator system used for waste heat recovery, Appl. Energy (2020), doi: 10.1016/j.apenergy.2020.115181.

[109] D. Rowe, Thermoelectrics Handbook: Macro to Nano, Taylor & Francis Group, NY, USA, 2018.

[110] X. Lu, X. Yu, Z. Qu, Q. Wang, T. Ma, Experimental investigation on thermoelectric generator with non-uniform hot-side heat exchanger for waste heat recovery, Energy Convers. Manage. 150 (2017) 403–414, doi: 10.1016/j.enconman.2017.08.030.

[111] A. Griesmar, "COMSOL Blog," 2013 . [Online]. Available: https://uk.comsol.com/blogs/what-is-comsol-multiphysics/. [Accessed 02 02 2020].

[112] COMSOL, "Introduction to Comsol Multiphysics," U.S. Patents, 2011.

[113] O. Isreallbeagwu, Modelling and comprehensive analysis of TEGs with diverse variable leg geometry, Sience Direct (2019), doi: 10.1016/j.energy.2019.05.088.

[114] L. Fan, G. Zhang, R. Wang, K. Jiao, A comprehensive and time-efficient model for determination of thermoelectric generator length and cross-section area, Energy Convers. Manage. 122 (2016) 85–94, doi: 10.1016/j.enconman.2016.05.064.

[115] W.-H. Chen, Y.-X. Lin, Y.-B. Chiou, Y.-L. Line, X.-D. Wang, A computational fluid dynamics (CFD) approach of thermoelectric generator (TEG) for power generation, Appl. Therm. Eng. 173 (2020), doi: 10.1016/j.applthermaleng.2020.115203.

[116] E. Massaguer, A. Massaguer, T. Pujol, J.R. Gonzalez, L. Montoro, Modelling and analysis of longitudinal thermoelectric energy harvesters considering series-parallel interconnection effect, Energy 129 (2017) 59–69, doi: 10.1016/j.energy.2017.04.061.

[117] E. Massaguer, A. Massaguer, L. MontoroJ, R. Gonzalez, Modeling analysis of longitudinal thermoelectric energy harvester in low temperature waste heat recovery applications, Appl. Energy (2015) 184–195, doi: 10.1016/j.apenergy.2014.12.005.

[118] S. Lineykin, S. Ben-yaakov, User-friendly and intuitive graphical approach to the design of thermoelectric cooling systems, Int. J. Refrig. 39 (2010), doi: 10.1016/j.ijrefrig.2006.12.004.